European Journal of Medicinal Chemistry 245 (2023) 114923

Contents lists available at ScienceDirect

European Journal of Medicinal Chemistry

journal homepage: www.elsevier.com/locate/ejmech

Bifunctional carbazole derivatives for simultaneous therapy and fluorescence imaging in prion disease murine cell models

Matteo Staderini [a,1], Silvia Vanni [b,1,2], Arianna Colini Baldeschi [b,3], Gabriele Giachin [c], Marco Zattoni [b], Luigi Celauro [b], Chiara Ferracin [b], Edoardo Bistaffa [d], Fabio Moda [d], Daniel I. Pérez [e], Ana Martínez [e,f], M. Antonia Martín [g], Olmo Martín-Cámara [a], Ángel Cores [a], Giulia Bianchini [a], Robert Kammerer [h], J. Carlos Menéndez [a,*], Giuseppe Legname [b,**], Maria Laura Bolognesi [i,***]

[a] Unidad de Química Orgánica y Farmacéutica, Departamento de Química en Ciencias Farmacéuticas, Facultad de Farmacia, Universidad Complutense, 28040, Madrid, Spain
[b] Laboratory of Prion Biology, Department of Neuroscience, Scuola Internazionale Superiore di Studi Avanzati (SISSA), via Bonomea, 265, 34136, Trieste, Italy
[c] Department of Chemical Sciences (DiSC), University of Padua, Via F. Marzolo 1, 35131, Padova, Italy
[d] Unit of Neuropathology and Neurology 5, Fondazione IRCCS Istituto Neurologico Carlo Besta, Via Celoria 11, 20133, Milano, Italy
[e] Centro de Investigaciones Biológicas Margarita Salas, CSIC, C. Ramiro de Maeztu, 9, 28040, Madrid, Spain
[f] Centro de Investigación Biomédica en Red en Enfermedades Neurodegenerativas, Instituto de Salud Carlos III, C. de Melchor Fernández Almagro, 3, 28029, Madrid, Spain
[g] Unidad de Química Analítica, Departamento de Química en Ciencias Farmacéuticas, Facultad de Farmacia, Universidad Complutense, 28040, Madrid, Spain
[h] Friedrich-Loeffler-Institut Bundesforschungsinstitut für Tiergesundheit, Federal Research Institute for Animal Health, Südufer 10, 17493, Greifswald, Insel Riems, Germany
[i] Department of Pharmacy and Biotechnology, Alma Mater Studiorum - University of Bologna, Via Belmeloro 6, 40126, Bologna, Italy

ARTICLE INFO

Keywords:
Prions
Prion protein
GN8
Theranostics
Carbazoles

ABSTRACT

Prion diseases are characterized by the self-assembly of pathogenic misfolded scrapie isoforms (PrP^{Sc}) of the cellular prion protein (PrP^{C}). In an effort to achieve a theranostic profile, symmetrical bifunctional carbazole derivatives were designed as fluorescent rigid analogues of GN8, a pharmacological chaperone that stabilizes the native PrP^{C} conformation and prevents its pathogenic conversion. A focused library was synthesized *via* a four-step route, and a representative member was confirmed to have native fluorescence, including a band in the near-infrared region. After a cytotoxicity study, compounds were tested on the RML-infected ScGT1 neuronal cell line, by monitoring the levels of protease-resistant PrP^{Sc}. Small dialkylamino groups at the ends of the molecule were found to be optimal in terms of therapeutic index, and the bis-(dimethylaminoacetamido)carbazole derivative **2b** was selected for further characterization. It showed activity in two cell lines infected with the mouse-adapted RML strain (ScGT1 and ScN2a). Unlike GN8, **2b** did not affect PrP^{C} levels, which represents a potential advantage in terms of toxicity. Amyloid Seeding Assay (ASA) experiments showed the capacity of **2b** to delay the aggregation of recombinant mouse PrP. Its ability to interfere with the amplification of the scrapie RML strain by Protein Misfolding Cyclic Amplification (PMCA) was shown to be higher than that of GN8, although **2b** did not inhibit the amplification of human vCJD prion. Fluorescent staining of PrP^{Sc} aggregates by **2b** was confirmed in

* Corresponding author. Unidad de Química Orgánica y Farmacéutica, Departamento de Química en Ciencias Farmacéuticas, Facultad de Farmacia, Universidad Complutense, Madrid, Spain.
** Corresponding author. Laboratory of Prion Biology, Department of Neuroscience, Scuola Internazionale Superiore di Studi Avanzati (SISSA), Trieste, Italy.
*** Corresponding author. Department of Pharmacy and Biotechnology, Alma Mater Studiorum—University of Bologna, Via Belmeloro 6, I-40126 Bologna, Italy.
E-mail addresses: josecm@ucm.es (J.C. Menéndez), legname@sissa.it (G. Legname), marialaura.bolognesi@unibo.it (M.L. Bolognesi).
[1] These authors contributed equally.
[2] Osteoncology Unit, Bioscences Laboratory, IRCCS Istituto Romagnolo Per Lo Studio Dei Tumori (IRST) "Dino Amadori", Meldola, Italy.
[3] Department of Pathology and Experimental Therapeutics, Bellvitge University Hospital-IDIBELL, 08908 Hospitalet del Llobregat, Spain. Institute of Biomedicine (IBUB) of the University of Barcelona (UB), 08028 Barcelona, Spain.

https://doi.org/10.1016/j.ejmech.2022.114923
Received 3 November 2021; Received in revised form 20 May 2022; Accepted 8 November 2022
Available online 15 November 2022

living cells. **2b** emerges as an initial hit compound for further medicinal chemistry optimization towards strain-independent anti-prion compounds.

Abbreviations

ASA	amyloid seeding assay
BBB	blood-brain barrier
BCA	bicinchoninic acid
BSA	bovine serum albumin
CSF	cerebrospinal fluid
DMAP	4-dimethylaminopyridine
ET	energy transfer
GdnHCl	guanidine hydrochloride
ICT	intra- or intermolecular charge transfer
ITC	isothermal titration calorimetry
MTT	methylthiazolyldiphenyl-tetrazolium bromide
NIR	near-infrared
PAINS	pan-assay interference compounds
PAMPA	parallel artificial membrane permeation assay
PK	proteinase K
PMCA	protein misfolding cyclic amplification
PMSF	phenylmethylsulphonyl fluoride
PRMs	protein recognition motifs
PrP^{C}	cellular prion protein
PrP^{Sc}	scrapie prion protein
PVDF	polyvinylidene fluoride
RMSD	root-mean-square deviation of atomic positions
RT-QuIC	real-time quaking-induced conversion
ASA	amyloid seeding assay
sCJD	Creutzfeldt-Jakob disease
Tg	transgenic
TLC	thin layer chromatography
TPSA	topological polar surface area
TRITC	tetramethylrhodamine
TSE	transmissible spongiform encephalopathies
vCJD	variant form of the Creutzfeldt-Jakob disease

1. Introduction

Prion diseases, also known as transmissible spongiform encephalopathies (TSE), are a class of neurodegenerative disorders of the central nervous system (CNS) [1], characterized by the self-assembly of pathogenic misfolded scrapie isoforms (PrP^{Sc}) of the cellular prion protein (PrP^{C}). The progressive neuronal propagation and accumulation of PrP^{Sc} may damage neurons directly, whereas reduced availability of PrP^{C} may hinder its putative pathological functions, contributing to the underlying neurodegeneration. Multiple lines of evidence suggest that many neurodegenerative diseases are proteinopathies [2], sharing the core mechanism of self-propagating misfolded proteins that accumulate in the CNS and ultimately trigger neurodegeneration [3]. Such mechanism has been reported for amyloid beta (Aβ) in Alzheimer's disease (AD), although mostly in terms of increased neuronal damage, rather than transmission. Thus, although prion diseases in humans are quite rare – approximately 1–2 cases each million of population worldwide [4] – these disorders might serve as a prototype model for neurodegeneration [5]. In this perspective, current drug discovery in prion diseases attracts broad interest [6,7]. Moreover, PrP^{C} has been found to be enriched in subpopulations of tumor-initiating cells, providing evidence about the contribution of PrP to the proliferation of cancer cells as well [8].

To date no effective therapeutic strategy is available for prion diseases. In the last few decades, several compounds have been found not only to affect PrP^{Sc} accumulation in *in vitro* models, but also to prolong survival in TSE-infected animals [9,10]. However, only few compounds, such as quinacrine and pentosan polysulfate, have reached the clinical evaluation stage [11]. More recently, a trial with doxycycline in patients with the sporadic form of Creutzfeldt-Jakob disease (sCJD) has been conducted, although with no satisfactory results [12]. Importantly, prion diseases are phenotypically heterogeneous and the reason for this variability seems to be enciphered in the abnormal structure acquired by PrP^{Sc}, which gives rise to distinct prion strains [13]. This might explain, at least in part, the enormous attrition rate of new drug candidates.

Another major issue with prion diseases is the inability to secure early diagnosis, which is critical for effective therapeutic interventions [14]. The definitive diagnosis requires post-mortem examination of the brain aimed at detecting and characterizing the presence of PrP^{Sc}, along with other disease hallmarks including the spongiform changes and the astroglial activation. *In vivo* diagnosis relies on clinical, laboratory tests and instrumental examinations. However, it is challenging to formulate a definitive diagnosis when patients are alive. In the case of the variant form of Creutzfeldt–Jakob disease (vCJD), which appeared in humans after consumption of food products derived from cattle affected by bovine spongiform encephalopathy (BSE), PrP^{Sc} can be detected by brain or tonsil biopsies [15]. With the advent of amyloid seeding assay (ASA) methodologies [16], such as the Protein Misfolding Cyclic Amplification (PMCA) [17] and the Real-Time Quaking-Induced Conversion (RT-QuIC) [18], trace amounts of PrP^{Sc} can now be detected in peripheral tissues, thus providing a significant progress. In light of the sensitivity and specificity of RT-QuIC, the technique has now been included in the diagnostic criteria for human prion diseases [19]. To note, through PMCA PrP^{Sc} can be propagated (amplified) *in vitro* at the expenses of PrP^{C}. Thus, PMCA has been recently used as an anti-aggregation drug screening assay [20].

Despite these recent achievements, given the setbacks and clinical trial failures that have characterized recent drug development in prion diseases and other proteinopathies, the scientific community has been reconsidering traditional approaches and focusing on more innovative tools [21]. One of these emerging tools is theranostics, i.e., single chemical entities able to deliver therapy and diagnosis simultaneously. The theranostic design concept involves small molecules directed to a single interacting protein that is both the therapeutic target and the biomarker. This is the case for theranostic compounds developed to label and simultaneously inhibit fibrillar aggregates of Aβ in AD [21].

Considering that PrP^{Sc} aggregates are a neuropathological hallmark, and that fluorescence spectroscopy has proven suitable for *in vivo* studies, the development of fluorescent staining agents able to detect PrP^{Sc} would be of great interest. Fluorescence-based imaging has emerged as an increasingly important technique for monitoring proteinopathies, possessing some advantages with respect to nuclear imaging, including lower cost, no exposure to radioactivity, availability, and ease of operation [22,23].

In an attempt to combine both therapeutic and diagnostic efficacy in a single molecule, we designed and synthesized a small set of fluorescent carbazole derivatives inspired by the anti-prion drug candidate GN8 (**1**, Fig. 1) [24]. Importantly, **1** was shown to extend survival in TSE-infected mice, while nonclinical safety assessment showed safety at the

concentration necessary to exert anti-prion activity [25]. We envisaged that by rigidifying the diphenylmethane structural fragment of **1** into a carbazole, we could preserve biological activity while unleashing emission of fluorescence and thus obtain molecules potentially acting as both therapeutic tools and chemical sensors for prion protein.

2. Results and discussion

2.1. Design strategy

GN8 (**1**) is a small molecule discovered in 2007 by Kuwata and co-workers in the course of an *in silico* screening aimed to identify compounds targeting hot spots of PrP^C, formed by residues undergoing rearrangements between the native state and higher-energy conformations [24]. GN8, featuring a diphenylmethane scaffold and two 2-(1-pyrrolidinyl)acetamido groups, acts as a chemical chaperone that stabilizes the native PrP^C conformation and prevents its pathogenic conversion into the pathogenic PrP^{Sc} isoform. Compound **1** has shown great efficacy in inhibiting PrP^{Sc} production *in vitro* across different prion strains, and prolonging survival of TSE-infected mice [24]. Furthermore, structure−activity relationships (SAR) studies suggested conformational rigidity at the benzylic position as an important feature for lead optimization [26]. *N,N′*-([cyclohexylmethylene]di-4,1-phenylene)bis(2-[1-pyrrolidinyl]acetamide (Fig. S1), a rationally-designed, constrained derivative of **1** carrying both phenyl groups in the optimal orientation, slows down TSE progression in mouse and macaque animal models [27].

Against this background, we became interested in generating a new class of GN8-analogues that could combine therapeutic and diagnostic properties in a single molecule, thus acting as potential prion theranostics. To this end, we applied a scaffold hopping approach to manipulate the structure of **1**. Replacement of the central diphenylmethane core with a carbazole led to **2a** (Fig. 1). Following this apparently slight modification, the central core of the molecule becomes planar and aromatic, properties that also make it fluorescent, thanks to the extended delocalization of the electrons in the π-orbitals of the carbazole ring. Importantly, extended π-conjugated flat systems have been recognized as critical features for binding and interfering with amyloids, due to changes in fluorescence properties upon placement of the molecule into and parallel to the plane of abnormally folded proteins [23]. The choice of carbazole as the structural core of our molecules was prompted by its high native fluorescence and the fact that carbazole-based fluorophores have been developed for amyloid imaging [28]. Furthermore, the presence of a NH group with acidic behavior in the excited state coupled with two basic groups in the side chains potentially allows an inner electron transfer from donor to acceptor groups and hence changes in the luminescence properties due to energy transfer (ET) and intra- or inter-molecular charge transfer (ICT). From the pharmacological point of view, carbazole-based compounds have shown anti-prion activity in

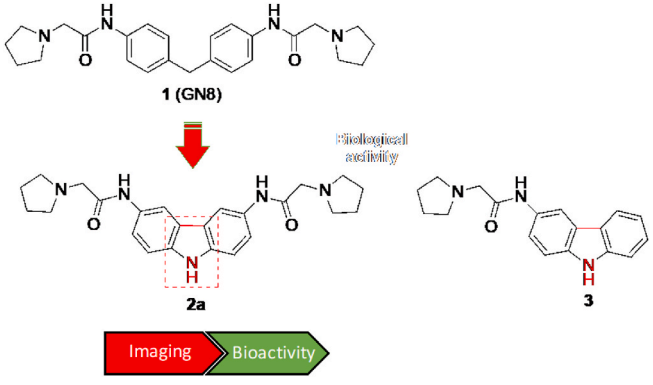

Fig. 1. Design of carbazole derivatives **2a** and **3** from GN8.

TSE-infected cells [29] and also the ability to mitigate amyloid neuropathology in a transgenic (Tg) mouse model of AD [30], confirming the promising role of a carbazole structure as pharmacological chaperone for proteinopathies.

This design strategy gives rise to structure **2a,** which, compared to the theranostics frequently obtained by conjugating two individual therapeutic and diagnostic fragments, shows the advantages of a lower molecular weight, and hence a potentially more favorable BBB permeation [21].

The symmetric compound **2a**, as well as GN8, can be viewed as a bivalent molecule endowed with two identical protein recognition motifs (PRMs) connected by the carbazole spacer. Such compounds can potentially interact simultaneously with two binding surfaces (hot spots) at the prion protein [31]. In order to verify the importance of the bivalent structure, we also planned the study of compound **3**, lacking one of the side chains (Fig. 1).

At this stage of our design, we became interested in verifying computationally whether compounds **2a** and **3** could be predicted to retain the prion protein-binding profile of GN8, despite the lower flexibility associated with its increased planarity. It is relevant to note that most mechanisms for reducing PrP^{Sc} levels involve prior binding to PrP^C, thereby halting its transformation into the PrP^{Sc} form. Therefore, the ability to bind PrP^C, which, unlike PrP^{Sc} whose structure is poorly defined [32], can be modeled computationally due to the existence of suitable protein 3D structures, is a highly relevant design criterion for anti-prion compounds [33].

Furthermore, many compounds that are able to bind to PrP^{Sc} are also PrP^C binders, as exemplified by Congo red [34] and quinacrine and its derivatives [35], and this is also true for antibodies. For these reasons, PrP^C targeting has been proposed as the anti-prion strategy that is closest to clinical application [27,36,37].

We performed docking studies to predict the binding mode of **2a** and **3** at mouse PrP^C, in comparison with **1**. **1** was placed in the hotspot determined by M129, G131, N159, V161, Y162, D178, C179, T183, I184, L185, H187, T190, G195, and E196 and the **1**-PrP^C complex was stabilized by two hydrogen bonds between the N159 NH amide backbone and the E196 carboxylic group. This binding pose was consistent with the NMR and calorimetric binding data previously provided by Kuwata, who also worked with mouse PrP^C [24]. A very similar pose was found for **2a**, interacting with the critical amino acid fragments placed into the binding site (N159 and E196). A minor difference was detected, namely that **2a** interacts with the E196 carboxylic acid through a hydrogen bond with the amide NH rather than an ionic bond with the pyrrolidine NH. The non-symmetric derivative **3** was placed in the hotspot and was stabilized by hydrophobic interactions, but no hydrogen bonds with N159 and E196 were found (Fig. 2A–C). In summary, both **2a** and **3** are predicted to bind PrP^C. In the case of the former compound, binding is mainly due to hydrogen bonding, while the latter interacts with the protein mainly by hydrophobic interactions within the hot spot region.

2.2. Synthesis

This computational study, together with the relatively accessible structure of **2a**, encouraged us to prepare a focused library around this motif as a part of a preliminary SAR study. The structural modifications carried out involved the replacement of the pyrrolidine group on the side chains with several secondary amino moieties (cyclic, acyclic and heterocyclic amines), providing derivatives **2a-i.** Our synthetic route is depicted in Scheme 1 and starts with the nitration of carbazole with a 1:1 mixture of acetic and nitric acid to give 3,6-dinitrocarbazole **4** and 3-nitrocarbazole **5** in moderate yields (20% of each compound). After separation, several literature methods for nitro reduction failed, but **4** was finally reduced in the presence of iron powder in a refluxing mixture of ethanol, water, acetic acid and 37% aqueous hydrochloric acid to give **6** in quantitative yield [38]. Compound **6** was then transformed into

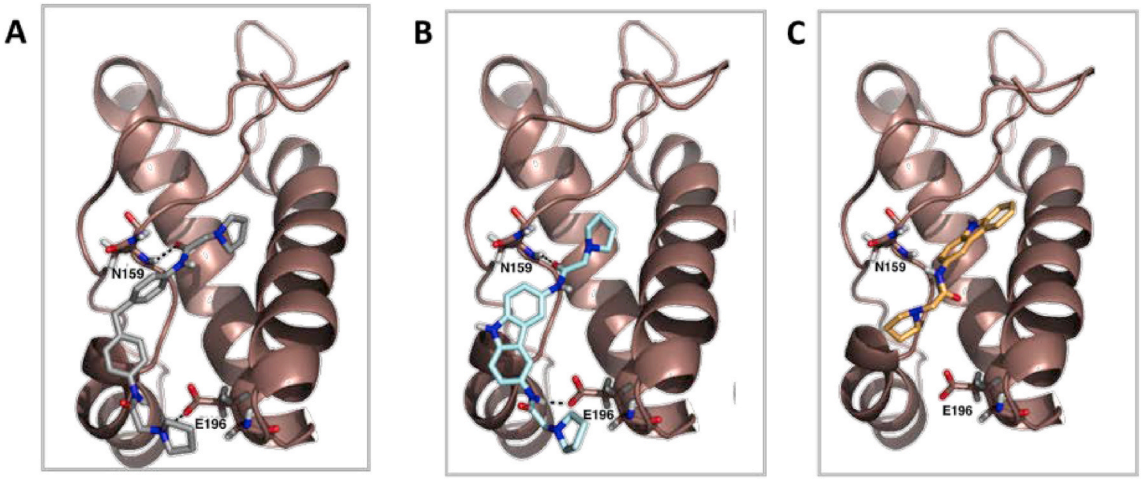

Fig. 2. Computational studies of the interaction of **2a** and **3** with PrP^C. **A-C.** Docking poses and their interactions with the critical PrP^C N159 and E196 amino acids, performed with AutoDock Vina from PDB 1AG2. The protocol was validated by GN8 docking. **A.** Compound **1** (GN8), shown in grey. **B.** Compound **2a**, shown in cyan. **C.** Compound **3**, shown in orange.

bis-halide **7** by double acylation with bromoacetyl bromide promoted by DMAP. With compound **7** in hand, we carried out its coupling reaction with different secondary amines in DMF at 80 °C during 24 h. Compounds **2** were obtained in yields ranging from 40 to 60%, which are acceptable considering the involvement of two reaction sites. A similar reaction sequence starting from 3-nitrocarbazole **5** successively afforded compounds **8** and **9**, the latter of which was treated with pyrrolidine to furnish **3**.

2.3. Fluorimetric study

We next investigated the photophysical properties of **2a** in several solvents (water, ethanol, cyclohexane, and acetonitrile) covering a broad range of polarities, as shown in Fig. 3 and Table 1. Generally speaking, the fluorescence properties (emission maxima and intensity) change by the effect of solvent polarity. In the case of compound **2a**, in organic solvents a fluorescence emission band is observed between 350 and 400 nm (λ_{ex} = 280 nm), varying according to solvent polarity. A band placed in the region of the near IR (NIR) (750–780 nm) appears in the polar protic or aprotic organic solvents but not in the non-polar solvent cyclohexane. This emission in the NIR region is weak in comparison to the principal emission because it is associated to intramolecular electron transfer [39], but it can nevertheless be successfully exploited for theranostic purposes due to the lower interference of surrounding tissue with NIR wavelengths. Interestingly, in aqueous media no emission is observed at the same concentration value. Similar changes in the fluorescence emission should be expected when **2a** is incorporated into misfolded proteins from an aqueous environment, allowing their selective detection.

2.4. Experimental study of the interaction of compound 2b with PrP^C

In order to verify experimentally the specific binding of compounds **2** to PrP^C, we initially attempted to assess the binding between compound **2b** and the $moPrP^C$ using an isothermal titration calorimetry (ITC) experiment. Unfortunately, the study could not be performed because at the conditions of the ITC experiment, $moPrP^C$ precipitates. For this reason, we chose a different approach based on the detection of spectral changes upon contact of **2b** and $moPrP^C$. For this study, we incubated both at equimolar concentrations at room temperature for 1h, followed by dialysis against PBS to eliminate the unbound excess. Subsequently, we measured the UV–Vis absorption spectrum of each dialyzed sample ($moPrP^C$ alone, compound **2b** alone and the incubated mixture). As shown in Fig. S2 (Supporting Information), **2b** shows a main absorption peak at 280 nm, which is coincident with the main absorption peak of the $moPrP^C$, and a broad decay of absorption from 300 to 450 nm, which we employed to detect the presence of the $moPrP^C$-bound compound, shown by an extra absorption tail-like contribution, absent in the spectrum of $moPrP^C$ alone. Taken together, these results represent a qualitative proof of the effective binding between the two molecules, supporting the computational analysis and the cellular assays and reinforces the rationale whereby the anti-prion compound **2** acts by a direct interaction with the prion protein.

2.5. Biological evaluation

Prior to its full biological characterization, drug-like properties of the library were studied computationally, using SwissADME [40]. As shown in Table S1, all compounds displayed TPSA (topological polar surface area) values below 110 $Å^2$ and suitable consensus $logP_{o/w}$, with no Lipinski violations or PAINS alerts. Gastrointestinal absorption and bioavailability were predicted to be good, as shown by the bioavailability radar (Fig. S2).

Furthermore, the blood-brain barrier (BBB) permeability of the library was evaluated on the *in vitro* parallel artificial membrane permeation assay (PAMPA-BBB). Some drugs with known ability (or lack thereof) to cross the BBB were used as positive and negative controls, respectively, which matched well those reported by Di et al. using the same method [41]. The results, which are shown in full detail in the Supporting Information (Table S2), show that only three of the compounds (**2e**, **2g**, **2h**) gave a clearly negative result.

Then, the therapeutic and diagnostic properties of compounds **2a-i** were assessed in *in vitro* models of prion diseases. Mammalian neuronal cell cultures, in which experimentally adapted rodent prion infection is stably maintained [42], have provided an efficient tool for phenotypic drug discovery [7]. In addition, such cell models proved to be versatile to study the theranostic potential of previously identified sets of styrylquinolines [43,44]. Their use is based upon the assumption that compounds with activity against experimentally adapted rodent prions will be active against naturally occurring prions, in particular those responsible for human diseases [45,46]. In this study, two prion-infected cell models were investigated, namely ScN2a, i.e., mouse neuroblastoma cells (N2a) infected with mouse-adapted scrapie strain RML or 22L, and ScGT1, i.e., immortalized murine hypothalamic neuronal cells infected with the same scrapie strains.

First, we sequentially assessed toxicity, anti-prion efficacy and imaging capabilities of **2a** in prion-infected cell culture models, in comparison with **1**. The cytotoxicity of different concentrations of **2a** (0.1-1-

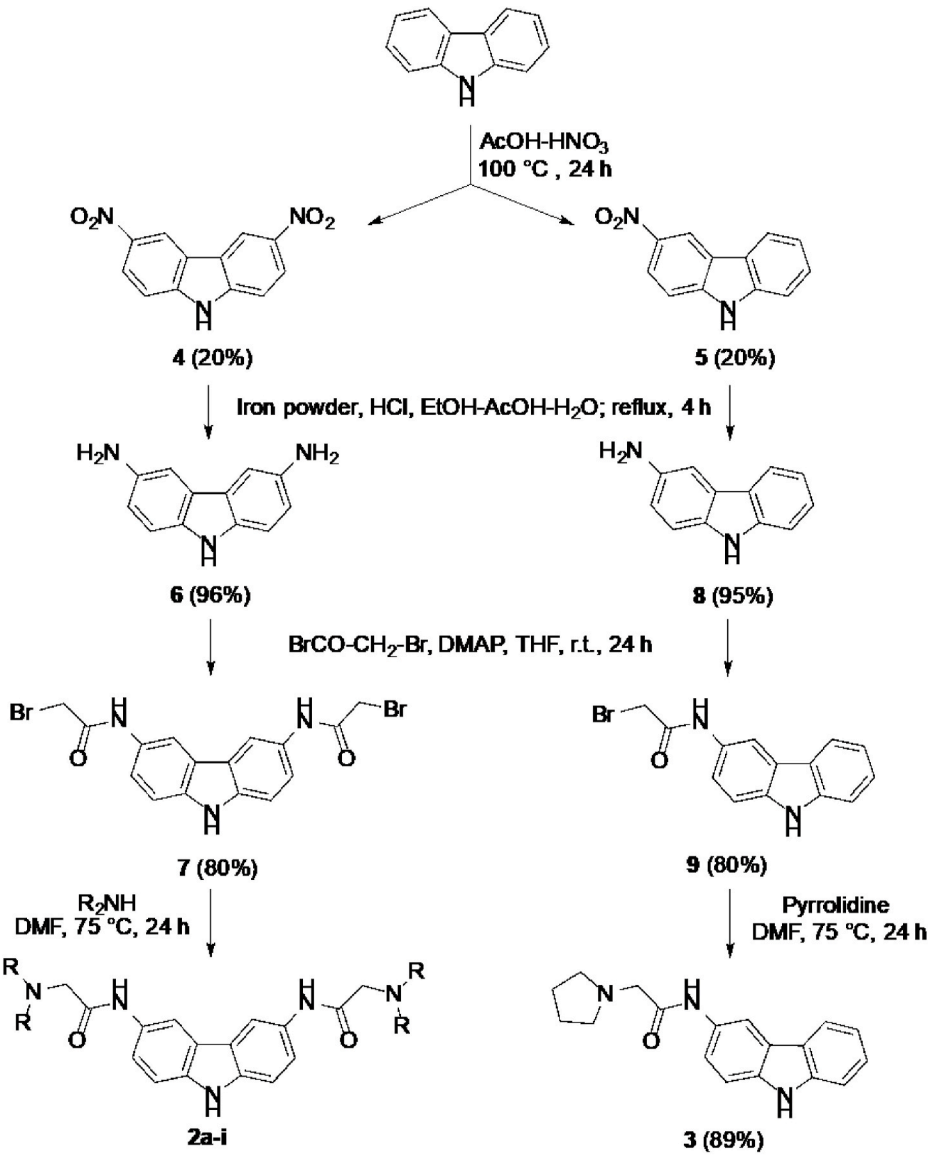

Cmpd	R_2N	Yield, %
2a	Pyrrolidin-1-yl	58
2b	Me_2N	60
2c	Et_2N	47
2d	i-Pr_2N	40
2e	Imidazol-1-yl	38
2f	Piperidin-1-yl	55
2g	Morpholin-1-yl	48
2h	N-Me-piperazin-1-yl	30
2i	N-Ph-piperazin-1-yl	40

Scheme 1. Synthetic route for the preparation of compounds **2a-i** and **3**.

10 μM) upon exposure for 5 days was determined using the MTT assay in RML-infected ScGT1 cells. The results of Fig. 4 show for **2a** a better toxicity profile than that of **1** at all tested concentrations.

Then, the anti-prion activity was assessed in RML-infected ScGT1 neuronal cell line, by monitoring the levels of protease-resistant PrP^{Sc} using proteinase K (PK) digestion, followed by Western Blotting. Effective concentrations for half-maximal inhibition (EC_{50}) of PrP^{Sc} formation were determined as we previously reported [44]. Remarkably, **2a** showed (Fig. 5) a dose-dependent anti-prion activity (EC_{50} = 7.4 μM), which was equipotent to that of **1** (EC_{50} = 7.8 μM). Thus, the molecular modification performed notwithstanding, **2a** is capable to effectively reduce PrP^{Sc} in chronically prion-infected cells in a manner similar to **1**, while being less cytotoxic.

Next, we investigated if **2a** could specifically detect PrP in mouse neuroblastoma cells infected with the same prion strain (RML-infected ScN2a). *In vitro* staining revealed the ability of **2a** (Fig. 6) to produce plaque-like fluorescence signals in ScN2a cells, indicating PrP labelling. Particularly, the compound gave a similar signal both in the presence

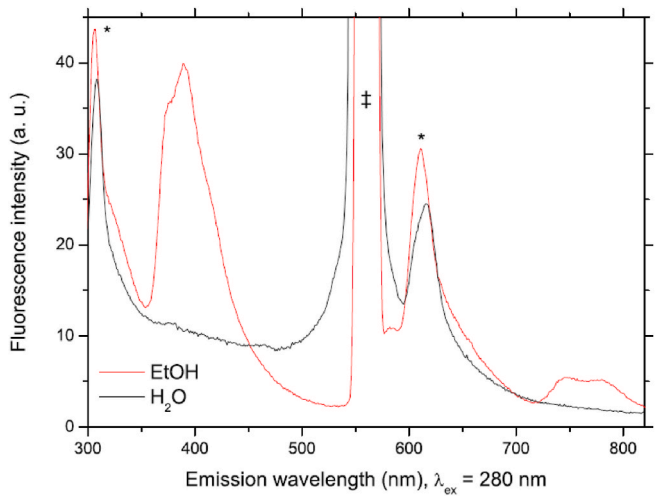

Fig. 3. Fluorescence spectra for **2** in solution with EtOH (red line) or water (black line).
Second-order light scattering is marked with ‡.

Table 1
Fluorescence excitation and emission maxima of **2a** in different solvents. The spectra were obtained at concentrations of 5.0×10^{-7} M (cyclohexane, ethanol and acetonitrile) and 1.0×10^{-6} M in water with the aim to detect fluorescence maxima. In all cases the emission spectra were recorded at $\lambda_{ex} = 280$ nm with the aim of comparing fluorescence intensity.

	Cyclohexane	Ethanol	Acetonitrile	Water
λ_{ex} (nm)	265, 280	269, 280	277, 280, 355	265, 280
λ_{em}(nm)	308, 604	315, 387, 605, 750, 784	309, 390, 609, 753	309, 385, 610,

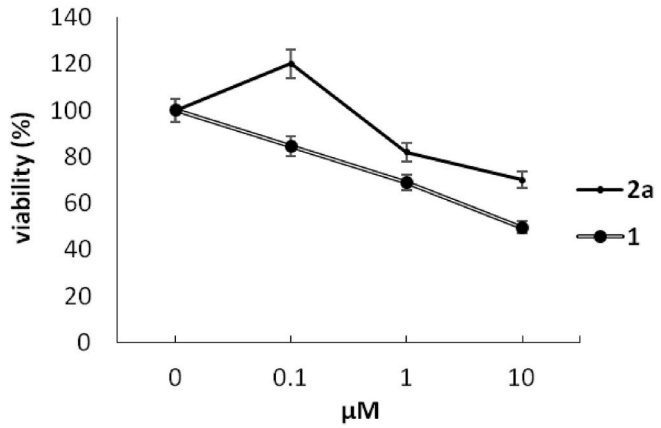

Fig. 4. Cell viability of ScGT1 RML cell lines treated with **2a** (solid black line) or **1** (double line). For each concentration tested, **2a** showed a lower toxicity compared to **1**. Interestingly, at 10 μM, **2a** continued to show a low toxicity, with a 70% residual cell viability.

and absence of protein denaturation with guanidine hydrochloride (GdnHCl), which suggests that **2a** is acting on PrP^{Sc} aggregates. In fact, as a strong denaturant, GdnHCl solubilizes aggregated proteins, allowing a discrimination of insoluble PrP^{Sc} strains. Since we observed a more intense signal in GdnHCl-treated ScN2a cells compared to untreated ones, and assuming that this increase in signal intensity comes from denatured PrP^{Sc} that became available to our compound after denaturation with GdnHCl, this experiment gives an indirect evidence of the effective binding between PrP^{Sc} and compound **2a**.

Based on the encouraging results found for **2a**, the complete library of carbazoles (**2a-i** and **3)** was assayed for the theranostic potential. For establishing anti-prion activity, all compounds were tested on RML-infected ScGT1 cells and then the cell lysates were tested for PrP^{Sc} by Western blot. Briefly, cells at confluence were split 1:10 and seeded in triplicate for each of the four conditions: no drug (vehicle), 0.1, 1 and 10 μM. The tested compound was added to the cell culture medium two days after seeding. After five days of treatment, cells were lysed, and lysates subjected to PK digestion (Table 2). The percentages of PrP^{Sc} remaining after digestion were measured in comparison to untreated ScGT1 lysates.

All compounds, with the sole exception of phenylpiperazine derivative **2i**, were effective in reducing PrP^{Sc} at the highest tested concentration (10 μM), with a reduction ranging from 26% to 83% (residual PrP^{Sc} from 17% for **2b** to 74% for **2e**). Five of the compounds – **2b**, **2c**, **2d**, **2h** and **3** – were effective also at 1 μM concentration, with PrP^{Sc} inhibition ranging from 39% to 75%. The homologous compounds **2b-2d** were the most potent within the series, indicating that the presence of an aliphatic tertiary amine is important for activity. On the other hand, as a positive control, we also tested the activity of **1**, and our results closely resembled those of Kuwata et al. [24], with a reduction in PrP^{Sc} levels of 87% at 10 μM. Calculated EC_{50} values for dimethylamino and diethylamino analogues **2b** and **2c** were similar (1.35 μM and 2.25 μM, respectively) (Fig. 7a).

In parallel, a MTT assay was performed for all the tested compounds to assess their cytotoxicity. Generally, an obvious dose-dependent ascending trend of toxicity was observed; interestingly, the two most effective compounds, **2b** and **2c**, showed low toxicity, with ≥90% cell viability after five days of treatment at all tested concentrations (Fig. 7B). These results make these two derivatives better than the original compounds **1** and **2a**, which show a higher toxicity (cell viability around 50–70%, respectively) at the EC_{50} value (Fig. 7B). While the monofunctional derivative **3** gave a good activity in terms of PrP^{Sc} reduction (residual PrP^{Sc} 26% at 10 μM, Table 2), we discarded the preparation of a second library of analogues derived from this simplified scaffold due to its higher cytotoxicity (29% of cell viability, Table 2). The combination of the activity and toxicity results suggest that simple dialkylamino groups at the ends of the molecule are optimal, and that the symmetrical bifunctional structure, while not essential for activity, leads to an improved therapeutic index. Not surprisingly, the ratio between the efficacious and toxic concentrations (therapeutic index) has been considered a critical feature for the drug-likeliness of anti-prion candidates [47].

To rule out that these derivatives might be able to affect PrP^{C} levels, **2b** and **2c** were also tested on non-infected GT1 cells, following the same protocol as for the ScGT1 cell line (Fig. 7C). None of the two compounds displayed a significant effect in altering PrP^{C} levels, a result of relevance for a potential use of these molecules, due to the involvement of PrP^{C} in many relevant physiological [48] and pathological functions, including the onset of AD [49]. We also tested **1**, and we observed a slight increase in PrP^{C} levels at all concentrations tested, with significance reached at 0.1 and 1 μM (Fig. 7C).

To corroborate our results, **1**, **2b** and **2c** screening was performed also with ScN2a RML cells obtaining similar results regarding cytotoxicity, except for the reference compound **1**, which showed a slight toxicity at the higher concentration (Fig. 7D). However, PrP^{Sc} clearance turned out to be slightly less effective, with EC_{50} being 6.6 μM for **2b**, 8 μM for **2c** and 2.5 μM for **1** (Fig. 7E).

Given that the mechanism by which the compound clears PrP^{Sc} is likely to involve its binding to the prion protein, we investigated the strain-dependency of the anti-prion effect. Prion strains, i.e., conformational variants of prion proteins, are associated with different clinical and pathological features, such as incubation time, lesion profiles and electrophoretic mobility [50].

To evaluate this aspect, we tested **2b** in ScGT1 and ScN2a cells infected with a different mouse-adapted prion strain, i.e., the 22L prion strain. The compound was able to reduce PrP^{Sc} in both 22L-infected cell

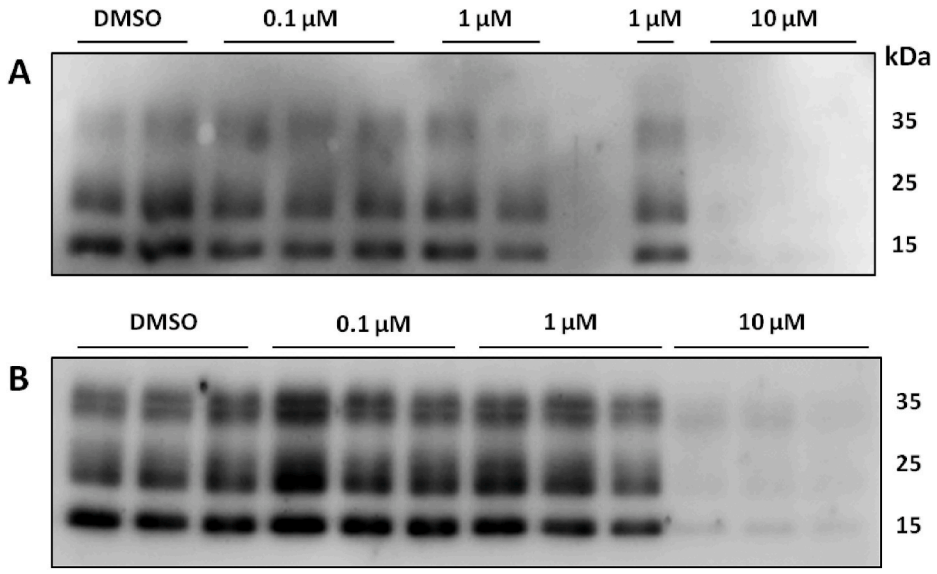

Fig. 5. Western blot analysis of PrP^{Sc} after 5 days of treatment of RML-infected ScGT1 cell line with **2a** (A) or **1** (B). PK digested cell lysates were probed with D18 antibody. Molecular weight is reported on the right (kDa).

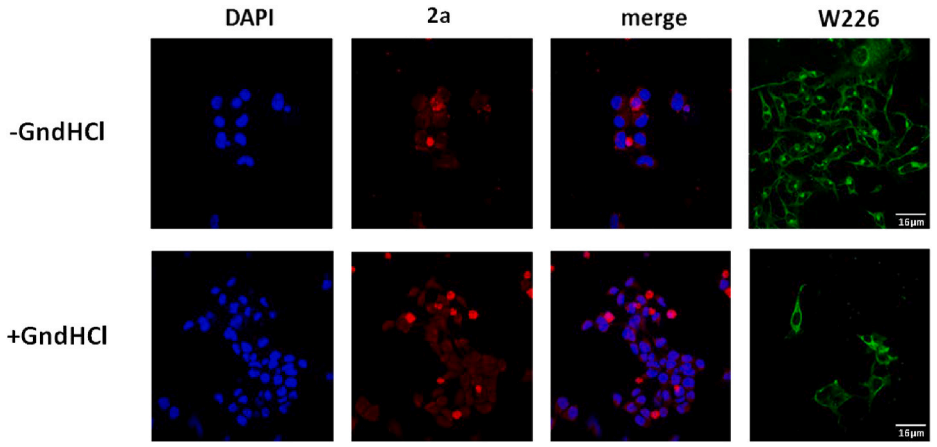

Fig. 6. Immunofluorescence and confocal microscopy analysis of **2a** in RML-infected ScN2a cell line. W226 antibody, which recognizes both isoforms, is used as positive control. Nuclei were stained with DAPI. Scale bar, 16 μm.

Table 2
Cell viability and PrP^{Sc} levels in RML-infected ScGT1 cells after 5 days of treatment with compounds **2a-i** and **3**.

Cmpd.	10 μM		1 μM		0.1 μM	
	% Cell viability	% PrP^{Sc} level	% Cell viability	% PrP^{Sc} level	% Cell viability	% PrP^{Sc} level
1 (GN8)	50	13	69	103	85	127
2a	71	27	85	103	118	148
2b	95	17	99	47	111	130
2c	103	31	99	57	108	84
2d	61	24	75	39	92	73
2e	77	74	89	98	100	120
2f	69	44	76	105	81	109
2g	84	59	86	102	101	96
2h	47	28	70	46	99	85
2i	63	134	73	136	71	124
3	29	26	72	75	83	78

lines, although with a different efficacy (Fig. 8). Indeed, in ScN2a 22L cells the calculated EC_{50} was 7.3 μM, while in ScGT1 22L it was 33.5 μM. These results show that **2b** is active against two different strains, even though with different potencies. This observation further expands the therapeutic potential of **2b**.

To gain further insight into the ability of **2b** to bind prion protein and inhibit PrP^{Sc} conversion, we performed an ASA experiment [16] with the full-length recombinant mouse PrP (MoPrP) in the presence of different concentrations of **2b**. While at equimolar concentrations (4 μM) **2b** did not show any effect on the MoPrP aggregation time (on average 21.5 h), at 20 μM and 40 μM **2b** delayed the aggregation of MoPrP by 5 and 9.5 h, respectively (Fig. 9). The collected data clearly

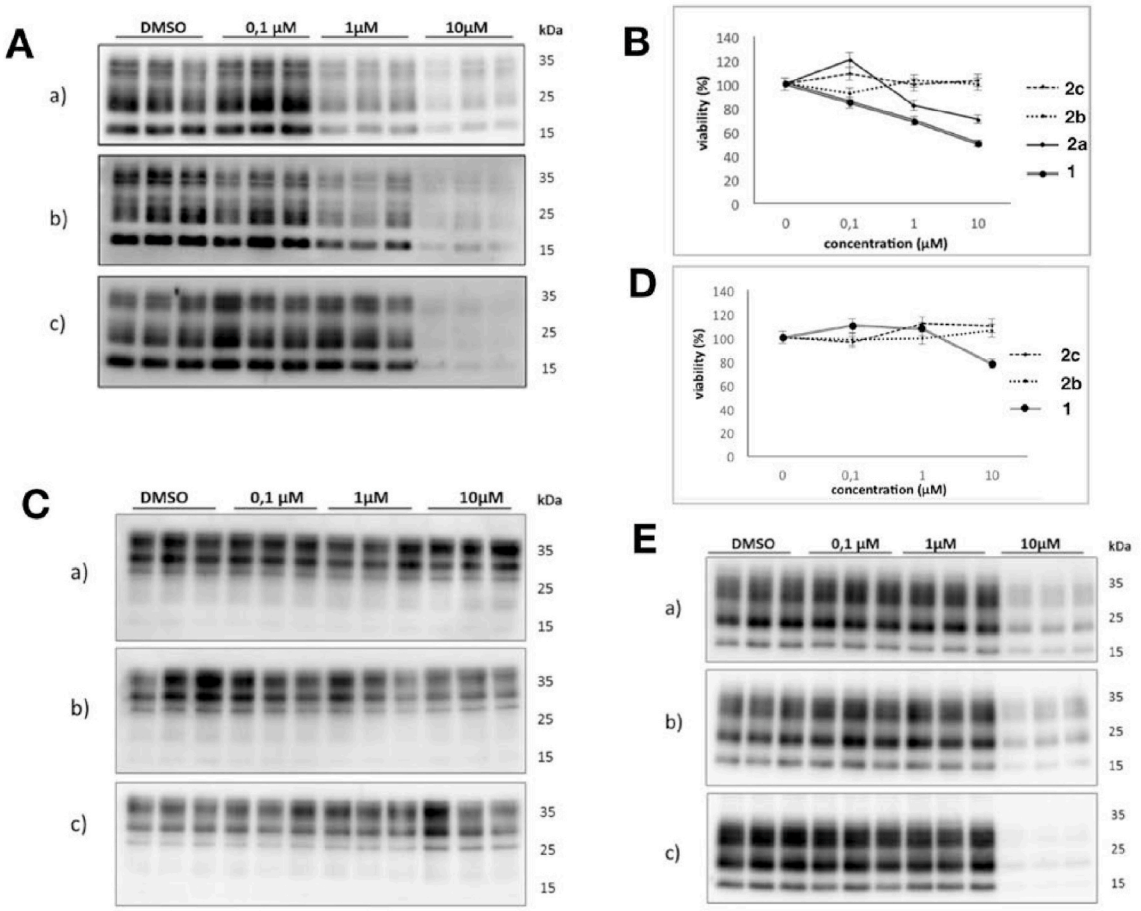

Fig. 7. **A**. Western Blot analysis of PrP^{Sc} after 5 days of treatment of ScGT1 RML cell line with **2b** (a), **2c** (b) or **1** (c). **B**. Cell viability of the ScGT1 RML cell line treated with **2c** (dashed line), **2b** (dotted line), **2a** (solid black line) or **1** (double line). **C.** Western Blot analysis of PrP^{C} after 5 days of treatment of GT1 cell line with **2b** (a), **2c** (b) or **1** (c). **D.** Cell viability of the ScN2a RML cell lines treated with **2c** (dashed line), **2b** (dotted line) or **1** (double line). **E.** Western Blot analysis of PrP^{Sc} after 5 days of treatment of ScN2a RML cell line with **2b** (a), **2c** (b) or **1** (c).

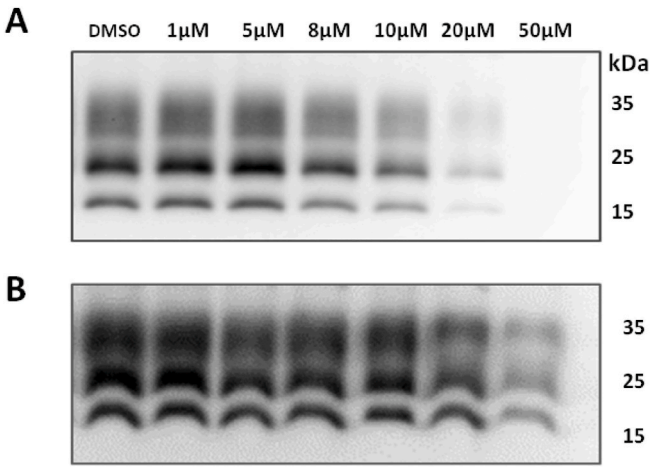

Fig. 8. Western Blot analysis of PrP^{Sc} after 5 days of treatment with **2b** in the ScN2a 22L cell line (A) or in ScGT1 22L (B). PK digested cell lysates were probed with D18 antibody. Molecular weight (in kDa) is represented on the right.

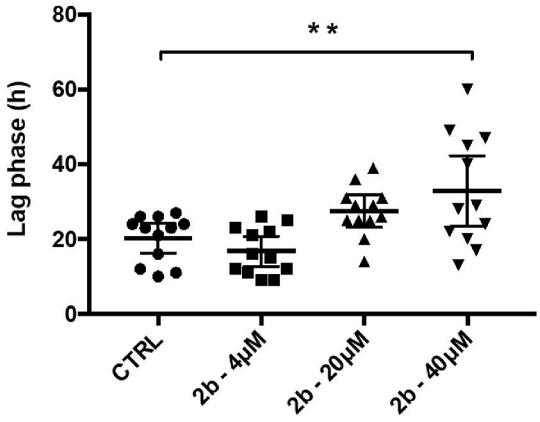

Fig. 9. Amyloid seeding assay. Prion protein fibril formation inhibitory activity *in vitro* for compound **2b.** Each bar represents the average of n = 12 replicates from 4 independent experiments. Bars denote standard error and median value (**$P < 0.005$).

point towards the ability of **2b** to bind the prion protein and exert a fibril-formation inhibitory activity.

We further investigated the ability of **2b** to prevent PrP^{Sc} formation and to interfere with the amplification of the mouse-adapted scrapie RML strain by PMCA, in comparison with **1**. As a source of PrP^{C}, we used the brain homogenates of wild type CD1 mice that were spiked with serial dilutions of RML prions. The results of Fig. 10A showed that the amplification of RML was completely inhibited by **2b** and only partially reduced by **1**. Remarkably, in the case of **2b**, none of the RML dilutions were detectable after PMCA, while in the case of **1**, two dilutions (10^{-5}

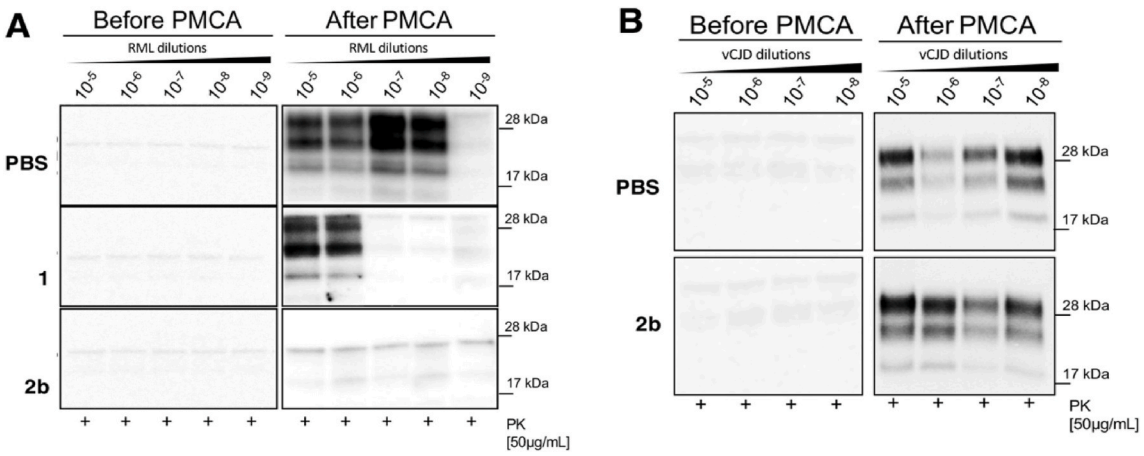

Fig. 10. A. Interference of compounds **1** and **2b** with the RML amplification by PMCA. Compound **2b** was able to completely block RML amplification while compound **1** exerted a limited inhibitory effect. No inhibition was observed in the PBS control conditions. **B.** Effect of compound **2b** on vCJD amplification by PMCA. All prion dilutions were efficiently amplified either in the presence or absence of compound **2b**, showing the inability of **2b** to interfere with vCJD amplification.

and 10^{-6}) were detected. As expected, the absence of both compounds (PBS conditions) led to the efficient amplification of almost all RML dilutions. Thus, **2b** was more efficient than parent compound **1** in inhibiting PrP^{Sc} formation induced by PMCA.

Based on these encouraging premises, we decided to confirm the anti-aggregating properties of **2b** in more clinically relevant assay conditions. We tested the efficiency of compound **2b** in interfering with the PMCA amplification of the human vCJD prion strain (Fig. 10B). In this case, contrary to the previous finding with mouse-adapted RML, compound **2b** did not inhibit the amplification of vCJD prion and all PrP^{Sc} dilutions could be detected after PMCA, thus indicating the presence of strain-specific activity. Species specificity of anti-prion drugs has already been reported for several compounds, including quinacrine, which has long been considered as the gold standard in prion drugs and has been also tested in clinical trials [46]. It is widely recognized that not all types of prions are equal, and that compounds found active against mouse prions *in vitro* are not necessarily effective against prions from other species [51]. Similarly, our results point out to the fact that the

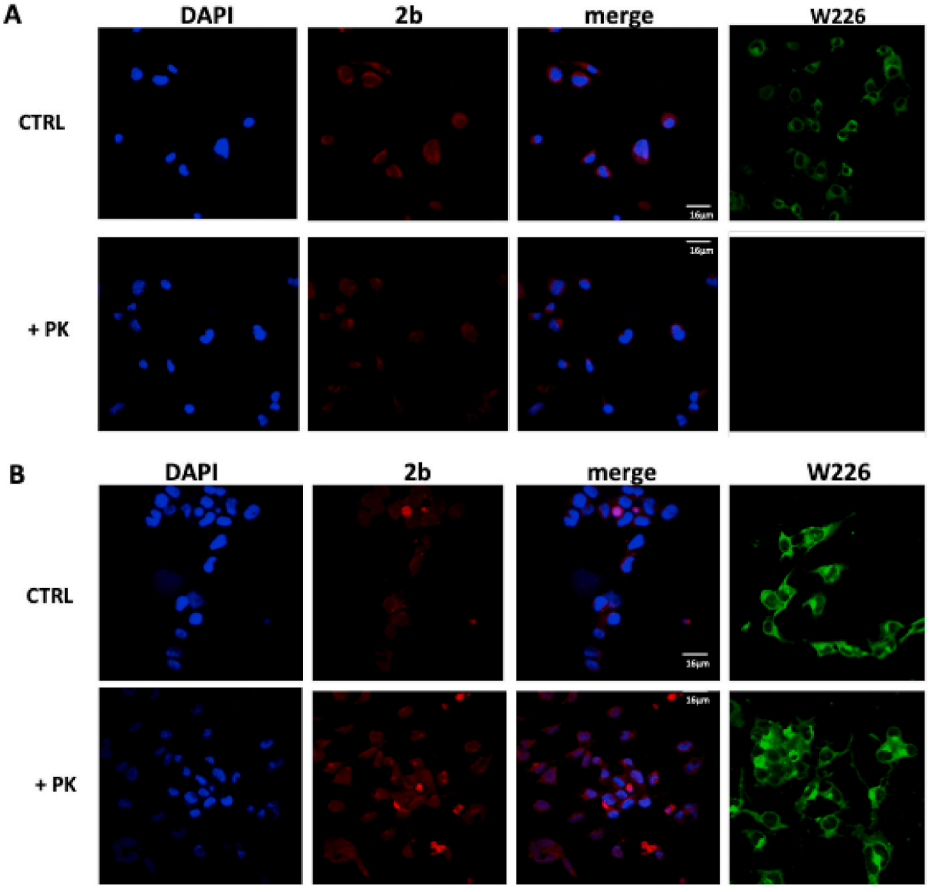

Fig. 11. Immunofluorescence and confocal microscopy analysis of **2b** in N2a (A) and ScN2a RML (B) cell lines. W226 antibody staining PrP is presented as positive control. Nuclei stained with DAPI. Scale bar, 16 µm.

available cell models replicating mouse-adapted prion strains, although representing a robust screening assay, do not precisely mirror the phenotype of the human pathological strains.

Indeed, the lack of a human cell culture able to stably replicate human prions is a major hurdle for prion drug discovery [52]. More complex cell culture models such as co-cultures of neurons, astrocytes, or other brain cell populations, as well as primary organotypic cultures obtained from brain slices, may represent a more accurate model of the real disease and therefore a more powerful tool to screen novel compounds in the future.

As part of the characterization of our compounds as theranostic agents, we tested the fluorescence properties of **2b** in both N2a and ScN2a RML cells, as previously done for **2a**. In uninfected N2a cells, **2b** only diffusely and mildly stains the cytoplasm without detectable protein clustering, whereas in infected cells **2b** apparently stains the formation of larger aggregates (Fig. 11B). The fact that the fluorescent foci were even more evident after proteinase K digestion seems to confirm that **2b** can bind and detect prion aggregates.

3. Conclusions

The generation of rigid compounds built around a carbazole core and bearing two identical dialkylaminoacetamido side chains has proved successful in leading to GN8 derivatives that maintain the anti-prion cellular profile of the parent compound, while showing concomitant imaging properties. Many of the synthesized carbazole analogues were able to induce a reduction in PrP^{Sc} levels on the RML-infected ScGT1 neuronal cell line. More importantly, the compounds are fluorescent and have been used to stain Pr^{Sc} proteins in cell models of the diseases, leading to an interesting theranostic cellular profile. Remarkably, the fluorescence properties have been achieved without the inclusion of any additional (large) fluorescent group, which could have hampered the pharmacokinetic properties. The dimethylamino derivative **2b**, which was the best-performing in terms of therapeutic index, exhibited improved pharmacological properties over GN8. Indeed, it effectively reduced prion load in two cell models infected with two murine prion strains (RML and 22L). In parallel, thanks to its fluorescent properties, it was able to stain prion aggregates in ScN2a RML cell line. Particularly, **2b** outperformed parent compound **1** in PMCA experiments. However, **2b** was not able to inhibit the amplification of human vCJD prion, bringing up the still unsolved need of non-murine cell models for prion drug discovery.

Collectively, these findings show the success of the proposed design strategy and suggest the dimethylamino derivative **2b** as a hit compound on which to build further medicinal chemistry efforts directed towards the identification of new derivatives able to deliver simultaneous therapy and fluorescence imaging against human strains.

4. Experimental section

4.1. Chemistry

4.1.1. General synthetic experimental information

All reagents (Aldrich, Fluka, SDS, Probus) and solvents (SDS), were of commercial quality and were used as received. 3,6-Diaminocarbazole **6** and 3-aminocarbazole **8** were synthesized using slightly modified literature procedures (see the Supporting Information). Thin layer chromatography (TLC) was performed on 0.20 mm silica gel 60 F254 plates (Merck, Germany), which were visualized by exposure to ultraviolet light (254 and 366 nm). Separations by flash chromatography were performed on silica gel (SDS 60 ACC 40–63 μm) or neutral alumina (Merck S22). Infrared spectra were recorded on a Nicolet IR 200 FT-IR spectrophotometer, with all compounds examined as KBr pellets or as thin films on NaCl disks. Nuclear magnetic resonance (NMR) experiments were run on were obtained on a Bruker Avance 250 spectrometer operating at 250 MHz for ^{1}H and 63 MHz for ^{13}C (CAI de Resonancia Magnetica Nuclear, Universidad Complutense). Spectra were acquired at 300 K, using DMSO-d_6 as solvent. Chemical shifts for ^{1}H and ^{13}C spectra were recorded using the residual non-deuterated solvent as the internal standard and are given in parts per million. Data are reported as follows: chemical shift (ppm), multiplicity (indicated as: s, singlet; br s, broad singlet; exch, exchangeable proton with D_2O; d, doublet; t, triplet; q, quartet; m, multiplet and combinations thereof), integrated intensity and coupling constants (*J*) in Hertz (Hz). Melting points were measured on a Reichert 723 hot stage microscope and are uncorrected. Absorption UV–Vis spectra were obtained with a Kontron Uvikon 810 UV–Vis double beam spectrophotometer. Corrected excitation and fluorescence spectra were obtained with a Fluoromax 4P spectrofluorometer controlled by FluorEssence 3.5 software for data acquisition. The slits were adjusted to 5 nm band pass. In both cases quartz cells with 1 cm of path of length were employed and all solvents used for these measurements were analytical or spectroscopic grade. Combustion elemental analyses were determined by the CAI de Microanalisis Elemental, Universidad Complutense. All final compounds showed ≥95% purity according to these microanalytical data.

***N,N'*-(9*H*-carbazole-3,6-diyl)bis(2-bromoacetamide) (7)**. A solution of 3,6-diaminocarbazole **6** (200 mg, 1.014 mmol), bromoacetyl bromide (0.511 g, 2.535 mmol) and DMAP (0.309 g, 2.535 mmol) in dry THF (10 mL) was stirred under argon for 24 h. The solvent was removed under reduced pressure and, after adding 2 M aqueous HCl (7 mL), the mixture was stirred for 1 h. The insoluble product was filtered, washed with water and dried overnight under reduced pressure in the presence of P_2O_5 to obtain **7** as a grey-brown solid (354 mg, 80%) that was sufficiently pure to be employed for the final step without further purification. ^{1}H NMR (250 MHz, DMSO) δ 11.22 (s, 1H), 10.41 (s, 2H), 8.39 (s, 2H), 7.48–7.56 (m, 4H), 4.09 (s, 4H) ppm. ^{13}C NMR (63 MHz, DMSO) δ 165.5 (2C), 134.6 (2C), 131.1 (2C), 122.6 (2C), 118.9 (2C), 116.9 (2C), 113.7 (2C), 31.4 (2C) ppm.

4.1.2. General procedure for the synthesis of compounds 2

To a stirred mixture of compound **7** (0.200 g, 0.445 mmol) in 2 mL of dry DMF was added two equivalents of the suitable secondary amine. The reaction mixture was stirred while heated at 75 °C for 24 h. The mixture was cooled, diluted with EtOAc (5 mL), washed with H_2O (3 x 2 mL) and a 10% KOH aqueous solution (2 mL), dried over anhydrous Na_2SO_4 and evaporated under reduced pressure to give compounds **2**.

***N,N'*-(9*H*-carbazole-3,6-diyl)bis(2-(pyrrolidin-1-yl)acetamide) (2a)**. Prepared from **7** (0.200 g, 0.445 mmol) and pyrrolidine (0.076 ml, 0.91 mmol); yield: 40%; reddish solid. Elemental analysis (%) calcd for $C_{24}H_{29}N_5O_2$: C 68.71, H 6.97, N 16.69; found: C 68.32, H 6.59, N 16.33. Mp: 169–172 °C. IR (KBr disk): 3399, 1654, 1560, 1492, 1228, 814 cm^{-1}. ^{1}H NMR (250 MHz, DMSO) δ 11.12 (br s, 1H), 9.78 (br s, 2H), 8.39 (s, 2H), 7.54 (d, J = 7.5 Hz, 2H), 7.42 (s, 2H), 3.38 (s, 4H, overlapped with the residual DMSO signal), 2.72 (s, 8H), 1.81 (s, 8H) ppm. ^{13}C NMR (63 MHz, DMSO) δ 168.0 (2C), 137.3 (2C), 130.7 (2C), 122.4 (2C), 119.5 (2C), 111.3 (2C), 108.9 (2C), 59.5 (2C), 54.2 (4C), 23.8 (4C) ppm.

***N,N'*-(9*H*-carbazole-3,6-diyl)bis(2-(dimethylamino)acetamide) (2b)**. Prepared from **7** (0.200 g, 0.445 mmol) and dimethylamine (0.046 ml, 0.91 mmol); yield: 58%; reddish solid. Elemental analysis (%) calcd for $C_{20}H_{25}N_5O_2$: C 65.37, H 6.66, N 19.06; found: C 65.09, H 6.31,N 19.35. Mp: 131–134 °C. IR (KBr disk): 3279, 1667, 1586, 868 cm^{-1}. ^{1}H NMR (250 MHz, DMSO) δ 9.71 (br s, 2H), 8.41 (s, 2H), 7.57–7.54 (m, 2H), 7.41–7.38 (m, 2H), 3.11 (s, 4H), 2.33 (s, 12H) ppm. ^{13}C NMR (63 MHz, DMSO) δ 168.5 (2C), 137.3 (2C), 130,7 (2C), 122.4 (2C), 119.5 (2C), 111.4 (2C), 111.2 (2C), 63.7 (2C), 45.8 (4C) ppm.

***N,N'*-(9*H*-carbazole-3,6-diyl)bis(2-(diethylamino)acetamide) (2c)**. Prepared from **7** (0.200 g, 0.445 mmol) and diethylamine (0.094 ml, 0.91 mmol); yield: 60%; brown solid. Elemental analysis (%) calcd for $C_{24}H_{29}N_5O_2$: C 68.06, H 7.85, N 16.53; found: C 67.8, H 7.55, N 16.44. Mp: 134–137 °C. IR (KBr disk): 3269, 2968, 1870, 1584, 1297, 808 cm^{-1}. ^{1}H NMR (250 MHz, DMSO) δ 9.65 (br s, 2H), 8.39 (d, J = 1.6

Hz), 7.58 (dd, $J = 8.7$, 1.9 Hz, 2H), 7.40 (d, $J = 8.6$ Hz, 2H), 3.18 (s, 4H), 2.65 (q, $J = 7.1$ Hz, 8H), 1.07 (t, $J = 7.1$ Hz, 12H) ppm. ^{13}C NMR (63 MHz, DMSO) δ 169.6 (2C), 137.3 (2C), 130.5 (2C), 122.5 (2C), 119.3 (2C), 111.3 (2C), 111.2 (2C), 57.9 (2C), 48.3 (4C), 12.4 (4C') ppm.

***N,N'*-(9*H*-carbazole-3,6-diyl)bis(2-(diisopropylamino)acetamide) (2d)**. Prepared from **7** (0.200 g, 0.445 mmol) and diisopropilamine (0.13 ml, 0.91 mmol); yield: 47%; brown solid. Elemental analysis (%) calcd for $C_{28}H_{41}N_5O_2$: C 70.11, H 8.62, N 14.60; found: C 69.90, H 8.37, N 14.34. Mp: 138–141 °C. IR (KBr disk): 3279, 2945, 1667, 1586, 1538, 868 cm^{-1}. ^{1}H NMR (250 MHz, DMSO) δ 11.14 (br s, 1H), 9.60 (br s, 2H), 8.36 (s, 2H), 7.62 (d, $J = 8.1$ Hz), 7.42 (d, $J = 8.1$ Hz, 2H), 3.13 (s, 8H), 1.08 (d, $J = 5.5$ Hz, 24H) ppm. ^{13}C NMR (63 MHz, DMSO) δ 171.09 (2C), 137.40 (2C), 130.30 (2C), 122.52 (2C), 119.14 (2C), 111.28 (2C), 111.23 (2C), 50.22 (2C), 50.09 (4C), 20.64 (8C) ppm.

***N,N'*-(9*H*-carbazole-3,6-diyl)bis(2-(1*H*-imidazole-1-yl)acetamide) (2e)**. Prepared from **7** (0.200 g, 0.445 mmol) and imidazole (0.077 g, 0.91 mmol); yield: 38%; brown solid. Elemental analysis (%) calcd for $C_{22}H_{19}N_7O_2$: C 63.91, H 4.63, N 23.72; found: C 63.53, H 4.48, N 23.34. Mp: 193–196 °C. IR (KBr disk): 3854, 1654, 1493, 1400, 1297, 814 cm^{-1}. ^{1}H NMR (250 MHz, DMSO) δ 10.38 (br s, 1H), 8.32 (s, 2H), 7.69 (s, 2H), 7.50–7.45 (m, 4H), 7.22 (s, 2H), 6.93 (s, 2H), 3.20 (s, 4H) ppm. ^{13}C NMR (63 MHz, DMSO) δ 166.0 (2C), 139.1 (2C), 137.8 (2C), 128.8 (2C), 122.9 (2C), 121.5 (2C), 119.7 (2C), 112.1 (2C), 112.0 (2C), 111.5 (2C), 50.1 (2C) ppm.

***N,N'*-(9*H*-carbazole-3,6-diyl)bis(2-(piperidin-1-yl)acetamide) (2f)**. Prepared from **7** (0.200 g, 0.445 mmol) and piperidine (0.089 ml, 0.91 mmol); yield: 55%; brown solid. Elemental analysis (%) calcd for $C_{26}H_{33}N_5O_2$: C 69.77, H 7.43, N 15.65; found: C 69.39, H 7.05, N 15.97. Mp: 161–164 °C. IR (KBr disk): 3278.0, 2933.1, 2811.4, 1664.6, 1584.6, 1533.4, 1492, 745.7, 642.7 cm^{-1}. ^{1}H NMR (250 MHz, DMSO) δ 10.74 (br s, 1H), 9.27 (br s, 2H), 8.01 (s, 2H), 7.16 (s, 2H), 7.04 (s, 2H), 3.00 (s, 4H), 2.13 (s, 8H), 1.22–0.84 (m, 12H) ppm. ^{13}C NMR (63 MHz, DMSO) δ 168.4 (2C), 137.3 (2C), 130.6 (2C), 122.5 (2C), 119.5 (2C), 111.4 (2C), 111.2 (2C), 63.1 (2C), 54.6 (4C), 25.9 (4C), 24.0 (2C) ppm.

***N,N'*-(9*H*-carbazole-3,6-diyl)bis(2-morpholinoacetamide) (2g)**. Prepared from **7** (0.200 g, 0.445 mmol) and morpholine (0.082 ml, 0.91 mmol); yield: 48%; brown solid. Elemental analysis (%) calcd for $C_{24}H_{29}N_5O_4$: C 63.84, H 6.47, N 15.51; found: C 63.67, H 6.17, N 15.55. Mp: 171–174 °C. IR (KBr disk): 3288, 1668, 1494, 1297, 911 cm^{-1}. ^{1}H NMR (250 MHz, DMSO) δ 11.08 (br s, 1H), 9.69 (br s, 2H), 8.34 (s, 2H), 7.50 (d, $J = 8.1$ Hz, 2H), 7.36 (d, $J = 8.5$ Hz, 2H), 3.33 (s, 8H), 3.12 (s, 4H), 2.47 (s, 8H) ppm. ^{13}C NMR (63 MHz, DMSO) δ 167.92 (2C), 137.3 (2C), 130.6 (2C), 122.4 (2C), 119.6 (2C), 111.6 (2C), 111.2 (2C), 66.5 (4C), 62.5 (2C), 53.7 (4C) ppm.

***N,N'*-(9*H*-carbazole-3,6-diyl)bis(2-(4-methylpiperazin-1-yl) acetamide) (2h)**. Prepared from **7** (0.200 g, 0.445 mmol) and 1-methylpiperazine (0.10 ml, 0.91 mmol); yield: 30%; reddish solid. Elemental analysis (%) calcd for $C_{26}H_{35}N_7O_2$: C 65.38, H 7.39, N 20.53; found: C 65.03, H 7.05, N 20.78. Mp: 185–188 °C. IR (KBr disk): 3409, 2948, 1654, 1542, 1492, 1459 cm^{-1}. ^{1}H NMR (250 MHz, DMSO) δ 11.20 (br s, 1H), 9.89 (br s, 2H), 8.43 (s, 2H), 7.55 (d, $J = 8.2$ Hz, 2H), 7.43 (d, $J =$ 8.7Hz, 2H), 3.55–3.11 (m, 10H), 2.79 (s, 6H) ppm. ^{13}C NMR (63 MHz, DMSO) δ 164.7 (2C), 137.4 (2C), 130.6 (2C), 122.4 (2C), 120.8 (2C), 111.4 (2C), 111.3 (2C), 65.3 (2C), 53.1 (4C), 49.9 (2C), 42.8 (4C) ppm.

***N,N'*-(9*H*-carbazole-3,6-diyl)bis(2-(4-phenylpiperazin-1-yl) acetamide) (2i)**. Prepared from **7** (0.200 g, 0.445 mmol) and 1-phenylpiperazine (0.14 ml, 0.91 mmol); yield: 40%; brown solid. Elemental analysis (%) calcd for $C_{36}H_{39}N_7O_2$: C 71.86, H 6.53, N 16.29; found: C 71.48, H 6.29, N 15.97. Mp: 176–179 °C. ^{1}H NMR (250 MHz, DMSO) δ 11.16 (br s, 1H), 9.87 (br s, 2H), 8.42 (s, 2H), 7.57 (d, $J = 8.3$ Hz, 2H), 7.42 (d, $J = 8.4$ Hz, 2H), 7.27–7.21 (m, 4H), 6.83–6.77 (m, 4H), 6.81 (d, $J = 7.0$ Hz, 2H), 3.28 (s, 12H), 2.81 (s, 8H) ppm. ^{13}C NMR (63 MHz, DMSO) δ 151.2 (2C), 137.4 (2C), 130.6 (2C), 129.3 (4C), 122.4 (2C), 119.9 (2C), 119.6 (2C), 119.3 (2C), 115.8 (4C), 111.6 (2C), 111.3 (2C), 53.0 (6C), 48.2 (4C) ppm.

2-Bromo-*N*-(9*H*-carbazol-3-yl)acetamide (9). A solution of compound **8** (0.100 g, 0.507 mmol), bromoacetyl bromide (0.102 g, 0.507 mmol) and DMAP (0.062 g, 0.507 mmol) in dry THF (10 mL) was stirred under argon for 24 h. When the reaction was completed, an aqueous solution of 2 M HCl (7 mL) was added, and the solution was stirred for 1 h. The resulting mixture was extracted with EtOAc (3 x 15 mL) and the combined organic layers were washed with water (3 x 15 mL) and dried over anhydrous Na_2SO_4. The resulting solution was evaporated *in vacuo* to obtain compound **9** (0,123 g, 80%) as a yellow-grey solid, which was sufficiently pure to be employed without further purification. ^{1}H NMR (250 MHz, DMSO) δ 11.28 (s, 1H), 10.45 (s, 1H), 8.44 (s, 1H), 8.08 (d, $J = 7.7$ Hz, 1H), 7.58–7.44 (m, 3H), 7.41 (t, $J = 7.6$ Hz, 1H), 7.17 (t, $J = 7.4$ Hz, 1H), 4.13 (s, 2H) ppm. ^{13}C NMR (63 MHz, DMSO) δ 165.2, 141.2, 137.5, 131.2, 126.6, 123.2, 123.0, 121.0, 119.7, 119.4, 112.1, 112.0, 111.9, 31.6 ppm.

***N*-(9*H*-carbazol-3-yl)-2-(pyrrolidin-1-yl)acetamide (3)**. Compound **9** (0.050 g, 0.114 mmol) and pyrrolidine (0.21 ml, 0.25 mmol) were refluxed in THF (8 mL) for 24 h. THF was removed *in vacuo* and the residue was diluted with EtOAc (5 ml) and successively washed with water (2 mL) and a 10% KOH aqueous solution (2 mL). The organic layer was dried over anhydrous Na_2SO_4 and evaporated under reduced pressure to give a yellow oil that was purified by chromatography on neutral alumina, eluting with EtOAc: petroleum ether (50:50), to isolate compound **3** as a yellow-grey solid in 89% yield. Elemental analysis (%) calcd for $C_{18}H_{19}N_3O$: C 73.69, H 6.53, N 14.32; found: C 73.32, H 6.57, N 13.95. Mp: 146–149 °C. IR (KBr disk): 3406, 3328, 2962, 1676, 1560, 817 cm^{-1}. ^{1}H NMR (250 MHz, d_6-acetone) δ 9.23 (br s, 1H), 8.62 (br s, 1H), 8.35 (d, $J = 1.8$ Hz, 1H), 8.07 (d, $J = 7.8$ Hz, 1H), 7.54 (dd, $J = 8.6$, 2.0 Hz, 1H), 7.41 (d, $J = 3.8$ Hz, 2H), 7.36–7.29 (m, 1H), 7.26–7.19 (m, 1H), 3.38 (s, 2H), 2.76–2.74 (m, 4H), 1.94–1.88 (m, 4H) ppm. ^{13}C NMR (63 MHz, d_6-acetone) δ 169.64, 140.7, 137.2, 130.4, 126.4, 123.9, 123.6, 121.0, 119.6 (2C), 112.5, 111.2, 111.2, 60.2, 55.1 (2C), 24.5 (2C) ppm.

4.2. Molecular modeling

4.2.1. Molecular docking

Docking studies were performed using AutoDock Vina, using the 121–231 amino acid residues of the NMR-resolved structure of mouse PrPC as a receptor (PDB: 1AG2). Ligands were created and minimized with ChemDraw and Chem3D. The grid box was placed in the hot-spot region and includes the residues M129, G131, N159, V161, Y162, D178, C179, T183, I184, L185, H187, T190, G195, and E196. The binding modes including an interaction with key residues N159 and E196. The protocol was validated by comparison between GN8 docking and the binding mode provided by Kuwata and co-workers (24). NMR and calorimetric binding data previously provided and the compared docking result and was consistent. The images from complexes between GN8, **2a** and **3** were obtained with PyMol 1.3.

4.3. Fluorescence studies

Fresh solutions were prepared in ethanol at 1.0×10^{-3} M concentration, and then appropriate aliquots of these solutions were taken and diluted in the solvent to be studied. The concentrations of the solutions measured by fluorimetry were 5.0×10^{-6} M or 1.0×10^{-6} M, meaning that the proportion of ethanol in the final solution was lower than 0.5%.

4.4. Biology

4.4.1. Production of recombinant 89–231 mouse PrP

pET-11a plasmid encoding for the mouse PrP 89–231 (moPrP 89–231) was expressed in *Escherichia coli* (*E.coli*) BL21 (DE3) cells (Stratagene). 100 mL of overnight culture was inoculated into Luria-Bertani medium complemented with 100 μg/mL ampicillin. At 0.6 OD_{600} the expression of the constructs was induced with 0.8 mM of isopropyl β-D galactopyranoside (IPTG). Cells were grown at 30 °C for

12 h and then lysed in 25 mM Tris-HCl, 5 mM EDTA, 0.8% TritonX100, pH 8.0 with fresh added 1 mM phenylmethylsulfonyl fluoride (PMSF) using PandaPLUS 2000 homogenizer (GEA Mechanical Equipment Italia S.p.A.). Inclusion bodies containing the recombinant proteins were washed several times in bi-distilled water and then dissolved in 8 M guanidine hydrochloride (GdnHCl) before loading onto a pre-equilibrated HiLoad 26/60 Superdex 200 pg column (Cytiva) and eluted in 5 M GdnHCl, 25 mM Tris-HCl, 5 mM EDTA, pH 8.0 at a flow rate of 2 mL/min. Proteins refolding was performed by dialysis against 20 mM sodium acetate, pH 5.5 using Spectrapor membrane. Purified proteins were analyzed by SDS-polyacrylamide gel electrophoresis under reducing conditions, dialyzed against phosphate buffer (PBS), pH 7.0 and stored at −80 °C. All chemicals used were purchased from Sigma-Aldrich.

4.5. Study of the interaction of 2b with PrP^C by UV–vis absorption spectroscopy

Ten μM of moPrP 89–231 was incubated at room temperature for 1 h with compound 2b at 10 μM (molar ratio 1:1) and then dialyzed against PBS pH 7.0 using Slide-A-Lyzer MINI Dialysis Devices, 3.5K MWCO (Thermo Fisher). Controls included 10 μM moPrP 89–231 and compound **2b** alone. Independent replicates ($n > 3$) of the experiments were carried-out. The UV–Vis absorption spectra (from 220 to 500 nm wavelength) of each of the dialyzed samples were measured with a Lambda XLS (PerkinElmer) spectrometer in 10 mm light path Quartz SUPRASIL® cuvette (Hellma).

4.6. Cell cultures

GT1 and RML-infected ScGT1 cells were cultured in Dulbecco's modified Eagle's medium (DMEM), supplemented with 10% of fetal bovine serum (FBS) and 1% penicillin-streptomycin. N2a and RML-infected ScN2a cells were cultured in Minimal Essential Medium (MEM) complemented with 10% FBS, 1% non-essential amino acids (NEAA), 1% L-glutamax and 1% penicillin-streptomycin.

4.7. MTT assay for cell viability

Cells were maintained in culture and grown to 80% confluence. The medium was refreshed, and the cells were detached. The cell density was adjusted to 2.5x10 [4] cell/mL with MEM (N2a, ScN2a) or 3x10 [4] with DMEM (GT1, ScGT1). The cell density was determined by cell counting using Scepter™ 2.0 Cell Counter (Millipore). Cells were seeded onto a 96-well, tissue culture-treated, clear bottom, plate (Costar) and the cells were allowed to settle for 24 h at 37 °C under 5% CO_2 prior to the addition of the compounds. Each compound – dissolved in DMSO- was diluted in the cell medium to a final concentration of 0.1, 1 and 10 μM. After 24 h, cell culture medium was refreshed together with the addition of the compound. The plate was incubated at 37 °C under 5% CO_2 for 5 days (N2a, ScN2a) or 7 days (GT1, ScGT1). The 3-(4,5-dimethylthiazol-2-yl)-2,5- diphenyltetrazolium bromide powder (MTT) (Sigma) was diluted in phosphate buffer solution (PBS) to a working dilution of 5 mg/mL. The medium was then removed, and the cells were incubated with the MTT solution for 3 h at 37 °C under 5% CO_2. After incubation, a solution of DMSO/2-propanol (1:1) was added to each well and the plate was kept at room temperature (rt) for 30 min before reading. The emission intensity was quantified using a Spectramax Gemini EM (SoftMax Pro) plate reader, excitation/emission ratio equal to 570/690 nm. MTT assays were performed in triplicate.

4.8. Drug treatment

All compounds were dissolved in 100% DMSO to a concentration of 10 or 20 mM. This solution was further diluted into a final stock solution of 1 mM with water. Confluent GT1 and ScGT1 cells were split 1:10 and three days after the drug (10 μM, 1 μM or 0.1 μM) was added to the medium for 7 days. Confluent N2a and ScN2a cells were split 1:10 and one day after the drug (10 μM, 1 μM, or 0.1 μM) was added to the medium for 5 days. Control cells were treated with the vehicle (≤0.001% DMSO). All the experiments were conducted in triplicates.

4.9. Western Blot for PrP detection

Cell lysis. After medium removal, cells were rinsed twice with cold PBS and 500 μL of lysis buffer (10 mM Tris-HCl pH 8.0, 150 mM NaCl, 0.5% Nonidet P-40, 0.5% deoxycholic acid sodium salt) was added directly to the cell plate. Cell lysates were centrifuged at 2000 rpm for 10 min at 4 °C in a bench microfuge (Eppendorf) and pellet was discarded. Total protein concentration was assessed with BCA assay (bicinchoninic acid method, Euroclone).

PK digestion of cell lysates. 500 μL of 1 mg/mL cell lysates were digested with 20 μg/mL of PK for 1 h at 37 °C. The reaction was stopped with 2 mM of phenylmethylsulphonylfluoride (PMSF) and the PK-digested cell lysates were centrifuged at 55000 rpm for 75 min at 4 °C in an ultracentrifuge (Beckman Coulter). The pellets were resuspended in 2X sample loading buffer (125 mM Tris HCl, pH 6.8, 10% 2-mercaptoethanol, 4% SDS, 0.2% bromophenol blue, 20% glycerol). For the non-PK digested sample, 50 μg of cell lysates were used and 5X loading buffer was added. All the samples were boiled for 10 min at 100 °C.

PK digestion of PMCA generated products. Ten μL of PMCA generated products was digested with 50 μg/mL of PK for 1 h at 37 °C under shaking. Reactions were stopped by boiling the samples previously supplemented with 7.5 μL of Bolt™ LDS sample buffer (Thermo Scientific).

SDS-PAGE and immunoblotting of cell lysates. Samples were loaded onto 15% Tris-Glycine SDS-PAGE gel and proteins were transferred onto a PVDF membrane (Millipore). The membrane was then blocked with 5% non-fat milk for 1 h at rt in continuous shaking and then incubated with 1 μg/mL anti-PrP Fab D18 at 4 °C overnight. After 3 washings with TBS-T (Tris 200 mM, NaCl 1,5 mM, 1% tween-20) the membrane was incubated with goat anti-human IgG F(Ab)2 conjugated with horseradish peroxidase (HRP) for 1 h at rt, continuous shaking. Blots were developed with enhanced chemiluminescent system (ECL, Amersham Biosciences) and visualized on Uvitec Alliance (Cambridge).

SDS-PAGE and immunoblotting of PMCA products. Samples were loaded onto 12% Bis-Tris Plus gel (Thermos Scientific) and subjected to SDS-PAGE. Proteins were then transferred onto PVDF membranes (Millipore) and immunoblotted overnight (4 °C under shaking) with the 6D11 antibody (Covance) after blocking with 5% non-fat dry milk. Membranes were then incubated with goat anti-mouse IgG F(Ab)2 conjugated with horseradish peroxidase (HRP) for 1 h at rt and finally developed with the enhanced chemiluminescent system (ECL Prime detection, Amersham) and visualized with the G:BOX Chemi Syngene system.

4.10. Detection of the in vitro effect of the synthesized compounds on prion fibril formation

Fibril formation was performed through ASA in accordance with the method previously described by Colby et al., with a few modifications [16]. Briefly, 16 μL of the diluted compounds at indicated concentrations were added to each well containing 184 μL of reaction solution including 100 μg/mL MoPrP (23–230), 2 M GdnHCl and 10 μM ThT in 1X PBS buffer in a 96-well black plate (BD Falcon). Each sample was performed in four replicates. Each well contained one 36 mm glass bead (Sigma). The plate was covered with sealing tape (Fisher Scientific), incubated at 37 °C with continuous shaking and read on SpectraMax M5 fluorescence plate reader (Molecular Devices) for 72 h by top fluorescence reading every 5 min at excitation of 444 nm and emission of 485 nm. Level of significance was calculated using unpaired Student t-test (2 tails, $p < 0.05$).

4.11. Immunofluorescence and confocal microscopy

The immunofluorescence microscopy experiments were performed as follows. Briefly, N2a and ScN2a cells were seeded to semi-confluence on glass coverslips for 24h. The cells were fixed with 4% paraformaldehyde, freshly prepared, for 15 min at rt and then permeabilized with 0.2% of TritonX 100 for 4 min at rt. Denaturation with 6 M GdnHCl for 10 min followed. After blocking with 1% bovine serum albumin (BSA) for 30 min at rt, the cells were incubated with 0.025% of compound (**3** or **2**) for 60 min. After washing several times with PBS, the primary antibody incubation followed (monoclonal antibody mAb W226 1:100) diluted in 1% of blocking buffer. After appropriate washing with PBS, fluorescently labelled secondary antibody incubation followed (Goat anti-mouse [GαMo]6 A594) for 1h at rt. For proteinase K digestion, ScN2a and N2a cells were grown on coverslips to semi-confluence. Twenty-four hours later cells were fixed with 4% paraformaldehyde for 10 min at rt and permeabilized with 0.2% of TritonX 100 for for 6 min at rt. Cells were incubated with PK (30 μg/ml) for 30 min at 37 °C. Digestion was stopped with 2 mM phenylmethylsulphonyl fluoride (PMSF, Sigma) for 15 min at rt. Cells were denatured with 6 M GdnHCl for 10 min. After blocking with 1% BSA for 30 min at rt, cells were incubated with primary and secondary Abs diluted in 1% BSA for 30 min at 37 °C. Images were acquired with a C1 confocal microscope (Nikon). FITC and TRITC filters were used for detection of PrP and compounds specific staining, while DAPI specific staining was acquired with 500 nm filter.

4.12. Protein Misfolding Cyclic Amplification (PMCA)

PMCA of RML and vCJD prions was performed as previously described [53,54], Briefly, PMCA substrates were prepared using brains of wild-type outbred CD-1 mice for RML amplification and brains of Tg mice expressing chimeric human-murine PrP sequence (Tg(MHu2M) FVB-B5378) for vCJD amplification. The study, including its ethical aspects, was approved by the Italian Ministry of Health. Brains were homogenized at 10% (weight/volume) in conversion buffer (PBS 1 × containing 150 mM sodium chloride and 1% Triton X-100) with the addition of complete protease inhibitor cocktail (Roche). For vCJD amplification, the substrate was supplemented with 0.05% of digitonin (Sigma). RML prions were diluted from 10^{-5} to 10^{-9} in CD1 substrates supplemented with (a) PBS, (b) 10 μM of compound **1** or (c) 10 μM of compound **2b**. Similarly, vCJD prions were diluted from 10^{-5} to 10^{-8} in Tg(MHu2M)FVB-B5378 substrates supplemented with PBS or 10 μM of compound **2b**. Each reaction mix was transferred into 0.2-mL PCR tubes, positioned on an adaptor placed on the plate holder of a micro-sonicator (Misonix, Model S3000) and subjected to PMCA reaction consisting of 29′ and 40″ sec of incubation at 37/40 °C and 20″ pulse of sonication set at potency of 260–270 W for RML amplification and 29′ and 20″ sec of incubation at 37/40 °C and 40″ pulse of sonication set at potency of 270–280 W for vCJD amplification. To increase the efficiency of the amplifications, three Teflon beads were added to each reaction tube.

Author contributions

MLB, GL and JCM conceived the study. MS and GB performed the synthesis and characterization of carbazole derivatives. SV performed all drug screening experiments and ASA assay. ACB performed immunofluorescence experiments. FB and EB performed PMCA analyses. DIP and AM performed the blood brain barrier permeation studies. CF and LC produced recombinant mouse PrP. GG and MZ conceived and performed the UV–Vis absorption spectroscopy assay. MAM performed the fluorimetry measurements. JCM and MLB supervised the synthesis. RK provided W226 antibody. AC and OM-C performed the computational studies, supervised by JCM. The manuscript was written through contributions of all authors. All authors have given approval to the final version of the manuscript.

Funding sources

Associazione Italiana Encefalopatie da Prioni (AIEnP) and Italian Ministry of Health (RRC), Italy. Ministerio de Ciencia e Innovación, Spain.

Declaration of competing interest

The authors declare that they have no known competing financial interests or personal relationships that could have appeared to influence the work reported in this paper.

Acknowledgements

This work was partially supported by Associazione Italiana Encefalopatie da Prioni (AIEnP) and the Italian Ministry of Health (RRC) to FM. Financial support from Ministerio de Ciencia e Innovación, Spain, through grants RTI2018-097662-B-I00 and PID2021-124983OB-I00 (to JCM) and PID2019-105600RB-I00 (to AM), is also gratefully acknowledged.

Appendix A. Supplementary data

Supplementary data to this article can be found online at https://doi.org/10.1016/j.ejmech.2022.114923.

References

[1] T.A. Bayer, Proteinopathies, a core concept for understanding and ultimately treating degenerative disorders? Eur. Neuropsychopharmacol 25 (5) (2015) 713–724.
[2] T.E. Golde, D.R. Borchelt, B.I. Giasson, J. Lewis, Thinking laterally about neurodegenerative proteinopathies, J. Clin. Invest. 123 (5) (2013) 1847–1855.
[3] G. Mallucci, Spreading proteins in neurodegeneration: where do they take us? Brain 136 (Pt 4) (2013) 994–995.
[4] C. Chen, X.P. Dong, Epidemiological characteristics of human prion diseases, Infect Dis Poverty 5 (1) (2016) 47.
[5] D.W. Sanders, S.K. Kaufman, B.B. Holmes, M.I. Diamond, Prions and protein assemblies that convey biological information in Health and disease, Neuron 89 (3) (2016) 433–448.
[6] S. Ghaemmaghami, M. Russo, A.R. Renslo, Successes and challenges in phenotype-based lead discovery for prion diseases, J. Med. Chem. 57 (16) (2014) 6919–6929.
[7] M.L. Bolognesi, G. Legname, Approaches for discovering anti-prion compounds: lessons learned and challenges ahead, Expert Opin. Drug Discov. 10 (4) (2015) 389–397.
[8] S. Martin-Lanneree, T.Z. Hirsch, J. Hernandez-Rapp, S. Halliez, J.L. Vilotte, J. M. Launay, S. Mouillet-Richard, PrP(C), From stem cells to cancer, Front. Cell Dev. Biol. 2 (2014) 55.
[9] A. Aguzzi, A.K.K. Lakkaraju, K. Frontzek, Toward therapy of human prion diseases, Annu. Rev. Pharmacol. Toxicol. 58 (2018) 331–351.
[10] A. Gandini, M.L. Bolognesi, Therapeutic approaches to prion diseases, Prog. Mol. Biol. Transl. Sci. 150 (2017) 433–453.
[11] A. Colini Baldeschi, S. Vanni, M. Zattoni, G. Legname, Novel regulators of PrP(C) expression as potential therapeutic targets in prion diseases, Expert Opin. Ther. Targets 24 (8) (2020) 759–776.
[12] S. Haik, G. Marcon, A. Mallet, M. Tettamanti, A. Welaratne, G. Giaccone, S. Azimi, V. Pietrini, J.R. Fabreguettes, D. Imperiale, P. Cesaro, C. Buffa, C. Aucan, U. Lucca, L. Peckeu, S. Suardi, C. Tranchant, I. Zerr, C. Houillier, V. Redaelli, H. Vespignani, A. Campanella, F. Sellal, A. Krasnianski, D. Seilhean, U. Heinemann, F. Sedel, M. Canovi, M. Gobbi, G. Di Fede, J.L. Laplanche, M. Pocchiari, M. Salmona, G. Forloni, J.P. Brandel, F. Tagliavini, Doxycycline in Creutzfeldt-Jakob disease: a phase 2, randomised, double-blind, placebo-controlled trial, Lancet Neurol. 13 (2) (2014) 150–158.
[13] R. Morales, P.P. Hu, C. Duran-Aniotz, F. Moda, R. Diaz-Espinoza, B. Chen, J. Bravo-Alegria, N. Makarava, I.V. Baskakov, C. Soto, Strain-dependent profile of misfolded prion protein aggregates, Sci. Rep. 6 (2016), 20526.
[14] R. Knight, Clinical diagnosis of human prion disease, Prog. Mol. Biol. Transl. Sci. 175 (2020) 1–18.
[15] R.G. Macfarlane, S.J. Wroe, J. Collinge, T.A. Yousry, H.R. Jäger, Neuroimaging findings in human prion disease, J. Neurol. Neurosurg. Psychiatry 78 (7) (2007) 664–670.
[16] D.W. Colby, Q. Zhang, S. Wang, D. Groth, G. Legname, D. Riesner, S.B. Prusiner, Prion detection by an amyloid seeding assay, Proc. Natl. Acad. Sci. U. S. A. 104 (52) (2007) 20914–20919.
[17] R. Morales, C. Duran-Aniotz, R. Diaz-Espinoza, M.V. Camacho, C. Soto, Protein misfolding cyclic amplification of infectious prions, Nat. Protoc. 7 (7) (2012) 1397–1409.

[18] R. Atarashi, K. Satoh, K. Sano, T. Fuse, N. Yamaguchi, D. Ishibashi, T. Matsubara, T. Nakagaki, H. Yamanaka, S. Shirabe, M. Yamada, H. Mizusawa, T. Kitamoto, G. Klug, A. McGlade, S.J. Collins, N. Nishida, Ultrasensitive human prion detection in cerebrospinal fluid by real-time quaking-induced conversion, Nat. Med. 17 (2) (2011) 175–178.
[19] A.J.E. Green, G. Zanusso, Prion protein amplification techniques, Handb. Clin. Neurol. 153 (2018) 357–370.
[20] M.E. Herva, S. Zibaee, G. Fraser, R.A. Barker, M. Goedert, M.G. Spillantini, Anti-amyloid compounds inhibit α-synuclein aggregation induced by protein misfolding cyclic amplification (PMCA), J. Biol. Chem. 289 (17) (2014) 11897–11905.
[21] M.L. Bolognesi, A. Gandini, F. Prati, E. Uliassi, From companion diagnostics to theranostics: a new avenue for Alzheimer's disease? J. Med. Chem. 59 (17) (2016) 7759–7770.
[22] V. Ntziachristos, Fluorescence molecular imaging, Annu. Rev. Biomed. Eng. 8 (2006) 1–33.
[23] M. Staderini, M.A. Martín, M.L. Bolognesi, J.C. Menéndez, Imaging of β-amyloid plaques by near infrared fluorescent tracers: a new frontier for chemical neuroscience, Chem. Soc. Rev. 44 (7) (2015) 1807–1819.
[24] K. Kuwata, N. Nishida, T. Matsumoto, Y.O. Kamatari, J. Hosokawa-Muto, K. Kodama, H.K. Nakamura, K. Kimura, M. Kawasaki, Y. Takakura, S. Shirabe, J. Takata, Y. Kataoka, S. Katamine, Hot spots in prion protein for pathogenic conversion, Proc. Natl. Acad. Sci. U. S. A. 104 (29) (2007) 11921–11926.
[25] J. Hosokawa-Muto, T. Kimura, K. Kuwata, Respiratory and cardiovascular toxicity studies of a novel antiprion compound, GN8, in rats and dogs, Drug Chem. Toxicol. 35 (3) (2012) 264–271.
[26] T. Kimura, J. Hosokawa-Muto, Y.O. Kamatari, K. Kuwata, Synthesis of GN8 derivatives and evaluation of their antiprion activity in TSE-infected cells, Bioorg. Med. Chem. Lett 21 (5) (2011) 1502–1507.
[27] K. Yamaguchi, Y.O. Kamatari, F. Ono, H. Shibata, T. Fuse, A.E. Elhelaly, M. Fukuoka, T. Kimura, J. Hosokawa-Muto, T. Ishikawa, M. Tobiume, Y. Takeuchi, Y. Matsuyama, D. Ishibashi, N. Nishida, K. Kuwata, A designer molecular chaperone against transmissible spongiform encephalopathy slows disease progression in mice and macaques, Nat. Biomed. Eng. 3 (3) (2019) 206–219.
[28] W. Yang, Y. Wong, O.T. Ng, L.P. Bai, D.W. Kwong, Y. Ke, Z.H. Jiang, H.W. Li, K. K. Yung, M.S. Wong, Inhibition of beta-amyloid peptide aggregation by multifunctional carbazole-based fluorophores, Angew Chem. Int. Ed. Engl. 51 (8) (2012) 1804–1810.
[29] T. Kimura, J. Hosokawa-Muto, K. Asami, T. Murai, K. Kuwata, Synthesis of 9-substituted 2,3,4,9-tetrahydro-1H-carbazole derivatives and evaluation of their anti-prion activity in TSE-infected cells, Eur. J. Med. Chem. 46 (11) (2011) 5675–5679.
[30] X. Wu, J. Kosaraju, W. Zhou, K.Y. Tam, SLOH, a carbazole-based fluorophore, mitigates neuropathology and behavioral impairment in the triple-transgenic mouse model of Alzheimer's disease, Neuropharmacology 131 (2018) 351–363.
[31] M. Staderini, G. Legname, M.L. Bolognesi, J.C. Menendez, Modulation of prion by small molecules: from monovalent to bivalent and multivalent ligands, Curr. Top. Med. Chem. 13 (19) (2013) 2491–2503.
[32] H. Wille, J.R. Requena, The structure of PrP(Sc) prions, Pathogens 7 (1) (2018).
[33] A. Kranjc, S. Bongarzone, G. Rossetti, X. Biarnes, A. Cavalli, M.L. Bolognesi, M. Roberti, G. Legname, P. Carloni, Docking ligands on protein surfaces: the case study of prion protein, J. Chem. Theor. Comput. 5 (9) (2009) 2565–2573.
[34] X.D. Cao Chen, Therapeutic Implications of Prion Diseases, 2020.
[35] C.E. Mays, S. Joy, L. Li, L. Yu, S. Genovesi, F.G. West, D. Westaway, Prion inhibition with multivalent PrPSc binding compounds, Biomaterials 33 (28) (2012) 6808–6822.
[36] M.L. Barreca, N. Iraci, S. Biggi, V. Cecchetti, E. Biasini, Pharmacological agents targeting the cellular prion protein, Pathogens 7 (1) (2018).
[37] A. Astolfi, G. Spagnolli, E. Biasini, M.L. Barreca, The compelling demand for an effective PrP(C)-Directed therapy against prion diseases, ACS Med. Chem. Lett. 11 (11) (2020) 2063–2067.
[38] A.M. Aleksandrov, R.P. Kashyap, T.J. Pehk, A.E. Petrenko, W.H. Watson, Synthesis of 1-substituted 12-oxahexacyclo[7.2.1.02,8.03,7.04,11.06,10]dodecanes and their transformation into pentacyclo[6.3.0.02,6.03,10.05,9]undecane derivatives, J. Org. Chem. 58 (7) (1993) 1831–1834.
[39] A.K. Das, S. Goswami, 2-Hydroxy-1-naphthaldehyde: a versatile building block for the development of sensors in supramolecular chemistry and molecular recognition, Sensor. Actuator. B Chem. 245 (2017) 1062–1125.
[40] A. Daina, O. Michielin, V. Zoete, SwissADME: a free web tool to evaluate pharmacokinetics, drug-likeness and medicinal chemistry friendliness of small molecules, Sci. Rep. 7 (2017), 42717.
[41] L. Di, E.H. Kerns, K. Fan, O.J. McConnell, G.T. Carter, High throughput artificial membrane permeability assay for blood-brain barrier, Eur. J. Med. Chem. 38 (3) (2003) 223–232.
[42] D. Vilette, Cell models of prion infection, Vet. Res. 39 (4) (2008) 10.
[43] M. Staderini, S. Aulic, M. Bartolini, H.N. Tran, V. Gonzalez-Ruiz, D.I. Perez, N. Cabezas, A. Martinez, M.A. Martin, V. Andrisano, G. Legname, J.C. Menendez, M.L. Bolognesi, A fluorescent styrylquinoline with combined therapeutic and diagnostic activities against Alzheimer's and prion diseases, ACS Med. Chem. Lett. 4 (2) (2013) 225–229.
[44] L. Zaccagnini, S. Brogi, M. Brindisi, S. Gemma, G. Chemi, G. Legname, G. Campiani, S. Butini, Identification of novel fluorescent probes preventing PrP (Sc) replication in prion diseases, Eur. J. Med. Chem. 127 (2017) 859–873.
[45] S. Brandner, Z. Jaunmuktane, Prion disease: experimental models and reality, Acta Neuropathol. 133 (2) (2017) 197–222.
[46] J. Bian, H.E. Kang, G.C. Telling, Quinacrine promotes replication and conformational mutation of chronic wasting disease prions, Proc. Natl. Acad. Sci. U. S. A. 111 (16) (2014) 6028–6033.
[47] B.C. May, A.T. Fafarman, S.B. Hong, M. Rogers, L.W. Deady, S.B. Prusiner, F. E. Cohen, Potent inhibition of scrapie prion replication in cultured cells by bis-acridines, Proc. Natl. Acad. Sci. U. S. A. 100 (6) (2003) 3416–3421.
[48] E. Biasini, J.A. Turnbaugh, U. Unterberger, D.A. Harris, Prion protein at the crossroads of physiology and disease, Trends Neurosci. 35 (2) (2012) 92–103.
[49] Y. Zhang, Y. Zhao, L. Zhang, W. Yu, Y. Wang, W. Chang, Cellular prion protein as a receptor of toxic amyloid-beta42 oligomers is important for Alzheimer's disease, Front. Cell. Neurosci. 13 (2019) 339.
[50] S.P. Mahal, C.A. Baker, C.A. Demczyk, E.W. Smith, C. Julius, C. Weissmann, Prion strain discrimination in cell culture: the cell panel assay, Proc. Natl. Acad. Sci. U. S. A. 104 (52) (2007) 20908–20913.
[51] S.H. Krance, R. Luke, M. Shenouda, A.R. Israwi, S.J. Colpitts, L. Darwish, M. Strauss, J.C. Watts, Cellular models for discovering prion disease therapeutics: progress and challenges, J. Neurochem. 153 (2) (2020) 150–172.
[52] Z. Krejciova, J. Alibhai, C. Zhao, R. Krencik, N.M. Rzechorzek, E.M. Ullian, J. Manson, J.W. Ironside, M.W. Head, S. Chandran, Human stem cell-derived astrocytes replicate human prions in a PRNP genotype-dependent manner, J. Exp. Med. 214 (12) (2017) 3481–3495.
[53] F. Moda, P. Gambetti, S. Notari, L. Concha-Marambio, M. Catania, K.W. Park, E. Maderna, S. Suardi, S. Haik, J.P. Brandel, J. Ironside, R. Knight, F. Tagliavini, C. Soto, Prions in the urine of patients with variant Creutzfeldt-Jakob disease, N. Engl. J. Med. 371 (6) (2014) 530–539.
[54] F. Moda, T.N. Le, S. Aulic, E. Bistaffa, I. Campagnani, T. Virgilio, A. Indaco, L. Palamara, O. Andreoletti, F. Tagliavini, G. Legname, Synthetic prions with novel strain-specified properties, PLoS Pathog. 11 (12) (2015), e1005354.